

## Two Galaxy Clusters: A3565 and A3560<sup>1</sup>

C.N.A. Willmer<sup>2,3,4,5</sup>, M.A.G. Maia<sup>2,3,4</sup>, S.O. Mendes<sup>3,6,7</sup>, M.V. Alonso<sup>8</sup>, L.A. Rios<sup>3,6</sup>, O.L. Chaves<sup>3,4</sup>, and D. F. de Mello<sup>4,9</sup>

Observatório Nacional, Rua General José Cristino 77, Rio de Janeiro, RJ 20921-030, Brazil

### ABSTRACT

We report 102 new redshifts and magnitudes for a sample of galaxies to  $R_F \sim 15.5$  mag in a  $2.17^\circ \times 2.17^\circ$  region centered on the galaxy IC 4296, the most luminous member of the A3565 cluster. Up to the limiting magnitude we find 29 cluster members, and measure a velocity dispersion of  $\sigma = 228 \text{ kms}^{-1}$ . The estimated total mass for this system is  $\sim 3.0 \times h^{-1} 10^{13} M_\odot$  (where  $h = H_0/100 \text{ km s}^{-1}\text{Mpc}^{-1}$ ), and its dynamical properties are quite typical of poor clusters presenting X-ray emission. We also find that galaxies with absorption lines are more concentrated towards the center of the cluster, while systems with emission lines are mainly located in the outer parts. The small velocity dispersion of the cluster, coupled to the known presence of an interacting pair of galaxies, and the large extent of the brightest cluster galaxy, could indicate that galaxy formation through mergers may still be underway in this system.

The surveyed region also contains galaxies belonging to the Shapley Concentration cluster A3560. Within 30 arc min of the cluster center, we detect 32 galaxies, for which we measure a velocity dispersion of  $588 \text{ kms}^{-1}$  and a mass of  $\sim 2 \times h^{-1} 10^{14} M_\odot$ . However, because our sample is restricted to galaxies brighter than  $M^*$ , these values should be considered only as rough estimates.

---

<sup>1</sup>Based on observations at Complejo Astronomico El Leoncito (CASLEO), operated under agreement between the Consejo Nacional de Investigaciones Científicas de la República Argentina and the National Universities of La Plata, Córdoba and San Juan; European Southern Observatory (ESO), partially under the ESO-ON agreement and Observatório do Pico dos Dias, operated by the Laboratório Nacional de Astrofísica (LNA).

<sup>2</sup>Visiting Astronomer, CASLEO, Argentina

<sup>3</sup>Visiting Astronomer, LNA, Brazil

<sup>4</sup>Visiting Astronomer, ESO, Chile

<sup>5</sup>Present address: UCO/Lick Observatory, University of California, 1156 High St., Santa Cruz, CA 95064

<sup>6</sup>Observatório do Valongo, UFRJ, Ladeira do Pedro Antônio 43, Rio de Janeiro, Brazil

<sup>7</sup>Present address: Department of Astronomy and Physics, Saint Mary's University, Halifax, NS, Canada B3H 3C3

<sup>8</sup>Observatorio Astronómico de Córdoba, Laprida 854, Córdoba, 5000, Argentina

<sup>9</sup>Present address: Space Telescope Science Institute, which is operated by the Association of Universities for Research in Astronomy, Inc. under contract to the National Science Foundation.

*Subject headings:* Galaxies: clusters: individual – galaxies: distances and redshifts – galaxies: photometry

## 1. Introduction

A region of the sky that presents a significant number of groups and clusters is the so called Centaurus Concentration (Lynden-Bell et al. 1989) which is a collection of about 20 groups and poor clusters which could be associated with the Great Attractor (Lynden-Bell et al. 1988). To date, only a few of these groups have been studied in detail (e.g., A3574 by Richter 1984; 1987; Willmer et al. 1991; and S753, Willmer et al. 1991; Jørgensen et al. 1995), being overshadowed by the much richer Shapley Concentration which lies in the background (e.g., Drinkwater et al. 1999; Bardelli et al. 1998; Ettori et al. 1997 and references therein).

Another reason for the paucity of studies of individual groups of galaxies in the region (as well as elsewhere) are the biases to which this kind of system is susceptible. In general, when analysing groups identified from the wide-angle redshift surveys (e.g., Huchra & Geller 1982; Maia et al. 1989; Nolthenius 1993; Garcia 1993; Ramella et al. 1999) one has to deal with two potential problems. The first is the variable limiting absolute magnitude of the group-finding algorithms (which is a function of redshift), so that typically only the brightest components are sampled. The second is the possibility that some of these groups are only chance projections along the line of sight rather than true physical associations, as only a few galaxies at most are assigned to the groups. The most effective means of overcoming these limitations is to probe the luminosity function of the groups to much fainter limits (e.g., Zabludoff & Mulchaey 1998a; Mulchaey & Zabludoff 1998a; Koranyi et al. 1998; Mahdavi et al. 1999), which allows not only establishing which galaxies are group members, but also ensures a more robust estimation of the group’s physical parameters (e.g., Zabludoff & Mulchaey 1998a).

In this work we present a redshift survey of a  $\sim 4$  square degrees region centered on IC 4296, which is the brightest galaxy of the cluster A3565, one of the groups belonging to the Centaurus Concentration. This cluster, located at R.A.  $13^h 33.8^m$  and Dec.  $-33^\circ 43'$  (1950.0) is classified as a Richness 1 cluster by Abell et al. (1989), and as a BM type I cluster by Brown & Burns (1991). The group associated with IC 4296 was first identified by Sandage (1972), and has been included in the group catalogues of Huchra & Geller (1982) (containing 3 galaxies) and Garcia (1993) (where it has 13). Most of the works dealing with this group have concentrated on IC 4296, which is the optical counterpart of the low-luminosity radio-source PKS 1333-33 (Mills et al., 1960; Killeen & Bicknell 1988). This galaxy also presents X-ray emission which has been studied by Forman et al. (1985) using *Einstein* data, and more recently by Buote & Fabian (1998) using *ASCA* data. The diffuse X-ray emission of the cluster detected by *ROSAT* has been studied by Mulchaey et al. (1996). The properties of several of its brighter members were investigated in a series of papers by Kemp & Meaburn (1991, 1993) and Kemp (1994). This cluster has also been used by Lauer & Postman (1994) and Lauer et al. (1998) in the study of peculiar velocities in the local Universe, and to estimate the far field Hubble constant. In the latter work, Lauer et al. (1998) have estimated the distance of IC 4296, the brightest cluster galaxy, as  $3220 \text{ kms}^{-1}$ .

The region surveyed in this work also includes A3560 ( $13^h 29.0^m$ ,  $-32^\circ 58'$ , 1950.0, Abell et al.

1989), who classified it as an irregular system of richness class 3, and estimated its redshift as  $cz \sim 3270 \text{ kms}^{-1}$ , the central position corresponding to that of the galaxy NGC 5193. In the analysis of the Shapley Concentration, Vettolani et al. (1990) noted that NGC 5193 and NGC 5193A are actually galaxies in the foreground of the cluster CE1329-327 identified by Melnick & Moles (1987), the center of which is  $14'$  off (mostly in Declination) from the Abell et al. (1989) position. From the measurement of ten spectra Melnick & Moles (1987) found that  $cz \sim 14850 \text{ kms}^{-1}$ , which places A3560 in the Shapley Concentration. That A3560 is a background cluster was also noted by Mould et al. (1991), though in their work they retain the name of A3560 to identify a foreground group (which contains some galaxies of A3565). Lauer et al. (1998) also refer to the distribution of galaxies at  $\sim 3800 \text{ kms}^{-1}$  centered on NGC 5193 as A3560. In this work we will assume that both NGC 5193 and NGC 5193A are part of A3565, and follow Vettolani et al. (1990) by calling A3560 the cluster in the Shapley Concentration. Other works dealing with this system have been Gregorini et al. (1994), who detected radio emission and showed that its peak originates from a position close to a dumbbell galaxy in the cluster; and Ebeling et al. (1996), Pierre et al. (1994) and Ettori et al. (1997), who analyse the X-ray emission detected by *ROSAT*.

This paper is organized as follows: the acquisition and observations of the galaxy sample are described in Section 2, followed by the analyses in Section 3. A summary of the main results follows in Section 4.

## 2. The Sample

### 2.1. Acquisition, Astrometry and Photometry

The sample of galaxies was defined from scans of an on-film copy of the ESO/Uppsala survey field 383 in the  $R$  band (IIIaF emulsion + GG630 filter, Lauberts & Valentijn 1989, hereafter ESO-LV) using the Observatório Nacional PDS 1010A microdensitometer. A square slit of  $20\mu\text{m}$  size was used, corresponding to  $1.35'' \times 1.35''$  projected on the sky, about  $0.25h^{-1} \times 0.25h^{-1}$  kpc at the cluster distance, where  $h = H_0/100 \text{ kms}^{-1} \text{ Mpc}^{-1}$ . We scanned an area of  $2.17^\circ \times 2.17^\circ$  ( $1.4h^{-1} \text{ Mpc} \times 1.4 h^{-1} \text{ Mpc}$ ) centered close to the position of IC 4296. The scanned area was divided into a mosaic of 9 scans each of  $2000 \times 2000$  pixels, with 100 pixels overlap between contiguous scans. This was done to minimize possible variations of the instrument focus due to the fact that we were not scanning a plate, while the overlap ensured that few objects on the border between scans, if any, would be lost, and would also allow a verification of the photometric stability. The scans were transformed into intensities in a procedure entirely analogous to that of Marston (1988) where the characteristic curve is derived comparing the surface brightness profiles of galaxies measured from the scans and CCD photometry. After the transformation into intensities, the scans were processed with FOCAS (Jarvis & Tyson 1981; Valdes 1982), and a possible candidate object was considered whenever it contained more than 9 contiguous pixels above the threshold, which we took as being  $3 \sigma$  above the sky level. Objects in common to one or

more scans were later used to shift the scans into the same instrumental magnitude system (e.g., Maddox et al. 1990).

The astrometric solution for each of the 9 individual scans was obtained independently. The first step was to identify in the object catalogue stars contained in the HST Guide Star Catalogue (Lasker et al. 1990, hereafter HSTGC). The positions of these stars were redetermined following the procedure of Assafin et al. (1997), using the PPM (Röser & Bastian 1991) and ACRS (Corbin & Urban 1988) catalogues. Basically, we selected PPM and ACRS stars in a  $2^\circ$  wide region centered on the individual scan, which were used to refine the HSTGC star positions, therefore defining the secondary reference frame with a rms error of  $\sim 0.5''$ . The secondary frame was then used to transform the scan  $x$  and  $y$  positions into right ascension and declination. We estimate that positional uncertainties should be smaller than  $1''$ .

The calibration used CCD photometry for 15 galaxies obtained during two observing runs at the LNA, the details of which are described in Table 1. The magnitudes were measured at three different isophotal levels, as described by Alonso et al. (1993). The calibrating galaxies are presented in Table 2 which shows in column (1) the galaxy identification used in this work, followed in column (2) by the previous identification when known; the  $R$  magnitudes and errors for each of the surface brightness levels 24, 25 and 26  $mag\ arcsec^{-2}$  are presented in columns (3), (4) and (5), and column (6) identifies the observing run described in Table 1. The magnitudes used in our catalogue, which we will denominate  $R_F$ , were obtained through a linear fit between the  $R_{25}$  and the instrumental photographic magnitudes. An estimate of the uncertainty of our  $R_F$  magnitudes was obtained by comparing our measurements with  $R_{25}$  of the ESO-LV catalogue for 25 galaxies in common. The comparison presented in Figure 1 shows that there is a mean difference  $R_F - R_{25}(ESO) = -0.05 \pm 0.24\ mag$ . For the 18 galaxies we have in common with Drinkwater et al. (1999) we find  $R_F - R_{DPP} = 0.11 \pm 0.25\ mag$ . Both comparisons suggest that our magnitudes have an average probable uncertainty of  $\sim 0.18\ mag$  if the errors are similar for each of the data sets.

The final catalog used to define the spectroscopic observations was limited at  $R_F = 15.5\ mag$  before making reddening corrections. In the analyses in Section 3, galaxy magnitudes were corrected for extinction using the DIRBE–IRAS maps of Schlegel et al. (1998) interpolated for the position of each galaxy, where we have assumed that  $A_{R_F} = A_R$ . In general the average reddening in the  $R$  band for this region is  $\sim 0.15\ mag$ .

## 2.2. Spectroscopy

The spectroscopic data used in this work were obtained at different telescopes, which are summarized in Table 3, where we identify the site (column 1), the telescope size (column 2), while the detector is identified in column (3) and its size in column (4); column (5) shows the grating rule, followed by the dispersion (column 6), resolution (column 7) and wavelength coverage

(column 8). The data were reduced in exactly the same manner as the SSRS2 data (da Costa et al. 1998), following the usual procedures of removing bias images, correcting by flatfield and making illumination corrections (e.g., Massey 1992), all within IRAF<sup>10</sup>. Radial velocities were measured using the RVSAO package (Kurtz et al. 1992; Kurtz & Mink 1998). In addition to the standard templates supplied with RVSAO, we used composite spectra of stars of various spectral types, a composite spectrum of galaxies measured for the SSRS (da Costa et al. 1989), and high signal-to-noise spectra of NGC 7507 and M31, the latter kindly supplied by V. de Lapparent and C. Bellanger. As in the case of the SSRS2 data (da Costa et al. 1998), which shared the same instrumental setups of the majority of observing runs reported herein, and was processed with the same software, the estimated velocity error for most spectra should be of the order of  $\sim 40 \text{ kms}^{-1}$ . An independent assessment of these errors can be made by comparing redshifts for 18 galaxies in common with Drinkwater et al. (1999), where we find a mean difference  $v - v_{DDP} = 40 \pm 87 \text{ kms}^{-1}$ . This result implies in  $\sim 61 \text{ kms}^{-1}$  uncertainty if both data sets have comparable errors, while if we consider the average uncertainty quoted by Drinkwater et al. (1999) for their measurements ( $67 \text{ kms}^{-1}$ ) this implies in an uncertainty of  $55 \text{ kms}^{-1}$  for our radial velocities. There are 6 galaxies in common with Quintana et al. (1995) for which we also measured radial velocities. We find a mean difference of  $v - v_{QRM} = 125 \pm 83 \text{ kms}^{-1}$ . The origin of this fairly large offset is unclear.

The final sample of galaxies is presented in Table 4<sup>11</sup> where we give in column (1) our object identification; in column (2) the previous identification obtained by matching galaxy positions with objects in the NED database, and for a few cases with the HSTGC, the original reference being identified in the footnotes; the right ascension and declination for epoch B1950.0 in columns (3) and (4) respectively and the  $R_F$  magnitudes in column (5). A rough morphological classification is shown in column (6), in a system consistent with that of da Costa et al. (1998), where T= -5 corresponds to ellipticals; -2 to S0s; 0 to S0/a; 5 to spirals in general; 16 to peculiar morphologies; 22 to dwarfs and 33 to galaxies with superposed stars. We should note that for fainter galaxies these classifications are uncertain because of the small apparent sizes. This is followed in column (7) by the heliocentric radial velocity; the estimated internal error (column 8); the number of emission lines used in the redshift determination (column 9) and the source code for the radial velocity (column 10), where s1, s2, etc. refer to the run number in Table 3, or the references shown in the table notes. In the table we have included all galaxies identified in this region to about  $R_F \sim 16.4 \text{ mag}$ . A total of 166 new observations are reported in this work, including the outer region discussed in Appendix A.

---

<sup>10</sup>IRAF is distributed by the National Optical Astronomy Observatories (NOAO) which is operated by the Association of Universities for Research in Astronomy, Inc. under contract to the U. S. National Science Foundation

<sup>11</sup>An electronic version of this table is available at [http://www.dan.on.br/other\\_surveys/a3565.html](http://www.dan.on.br/other_surveys/a3565.html)

### 3. Analysis

#### 3.1. Distribution of Galaxies

The sample of galaxies brighter than  $R_F = 15.5 \text{ mag}$  considered in this work is shown in Figure 2, where the symbols represent galaxies in different redshift intervals, as noted in the caption, while the symbol size is a function of the object magnitude. The most prominent features in this plot are A3560 at approximately  $13^h 30^m$  and  $-32^\circ 50'$ , at the upper right, and A3565 at  $13^h 33^m -33^\circ 40'$ , close to the center of the surveyed region. To the adopted magnitude limit, there are 111 galaxies, of which 110 (99%) have measured radial velocities. The distribution in radial velocities bins of  $250 \text{ kms}^{-1}$  is shown in Figure 3, where all velocities were corrected for galactic rotation through  $v_o = v_\odot + 300 \sin l \cos b$ . The two main peaks correspond to A3565 at  $\sim 3600 \text{ kms}^{-1}$  and galaxies associated with A3560 and the Shapley Concentration at  $\sim 15000 \text{ kms}^{-1}$ . The smaller peak at  $\sim 7000 \text{ kms}^{-1}$  is due to a group of 3 galaxies close to the position of IC 4296, plus a few other galaxies distributed over the whole field. This loose distribution of galaxies at  $\sim 7000 \text{ kms}^{-1}$  has also been detected by Drinkwater et al. (1999). In contrast, the structure at  $\sim 11000 \text{ kms}^{-1}$  found by those authors in the foreground of the Shapley Concentration is not very prominent in our sample; an inspection of their redshift maps suggests that most of the galaxies in that structure are located to the south of our survey.

#### 3.2. A3565

The peak corresponding to A3565 in Figure 3 contains 30 galaxies which are well separated in velocity space from the foreground galaxies at  $\sim 2000 \text{ kms}^{-1}$  and the background at  $\sim 7000 \text{ kms}^{-1}$ . Because the surveyed area is rather small ( $r < 0.7 h^{-1} \text{ Mpc}$ ), it is possible that some outlying galaxies are being lost (e.g., Mahdavi et al. 1999). This in fact is suggested when comparing the present catalogue with that derived by Garcia (1993) using the LEDA database (Paturel et al. 1991), which contains three galaxies beyond the survey boundaries. However, in order to keep our sample homogeneous and well defined, we have not considered in the analysis these possible member galaxies. In this work we will consider as group members only those galaxies that are within the surveyed area and with radial velocities within  $3 \sigma$  of the cluster mean (Yahil & Vidal 1977), where  $\sigma$  is the cluster velocity dispersion uncorrected for velocity errors. This eliminates WMMA 219 ( $v_\odot=4494 \text{ kms}^{-1}$ ) from the sample. The spatial distribution of likely member galaxies of A3565 is shown in Figure 4, where again we have coded the symbol size as a function of the apparent  $R_F$  magnitude of the galaxy, while crosses represent galaxies with emission lines in the spectra, and open squares galaxies only presenting absorption line spectra.

In Table 5 we present the dynamical properties of A3565, most of which were calculated using the “classical estimators” (mean radial velocity, velocity dispersion and mass), while the cluster centroid was estimated using an unweighted average. The velocity dispersion and errors

were derived following Danese et al. (1980), where the radial velocity uncertainty is accounted for, while for the other parameters we used the “jackknife” technique (e.g., Bothun et al. 1983). In the table we also show the values of the central location and scale estimates calculated using ROSTAT (Beers et al. 1990), the errors for the latter being estimated by means of 1000 bootstrap simulations. As may be seen in the table, the values of both classical and robust estimators agree very well. All these parameters were calculated without weighting by luminosity. The mean harmonic radius ( $R_h$ ), the mean pairwise separation ( $R_p$ ) and the virial mass ( $M_{VT}$ ) were calculated using the expressions of Ramella, Geller & Huchra (1989). The uncertainty for the latter was estimated using standard error propagation, which takes into account the uncertainty in  $\sigma$  and the jackknife error for  $R_h$ . We also calculate the projected mass ( $M_p$ ) which is an estimator proposed by Heisler, Tremaine & Bahcall (1985) that is less sensitive to the presence of interlopers. Both  $M_{VT}$  and  $M_p$  were shown by West, Oemler & Dekel (1988) to give reliable measures of the cluster mass.

The velocity dispersion of A3565 ( $228 \text{ kms}^{-1}$ ) is marginally higher than the typical value for groups of galaxies  $\sim 194 \text{ kms}^{-1}$  (Ramella et al. 1999), yet in the lower range of velocity dispersions measured by Zabludoff & Mulchaey (1998a) in their sample of 12 poor clusters with X-ray emission. The mass derived from the Virial Theorem in addition to the projected mass estimator by Heisler et al. (1985) are in good agreement, giving a mass of the order of  $3 \times 10^{13} M_\odot$ . The uncertainties for  $M_{VT}$  are of the order of 30%, a value which is consistent with that measured for simulated clusters by West et al. (1988). The estimated uncertainty measured for  $M_p$  is probably too small, as the latter authors found that it presents comparable errors to those of  $M_{VT}$ .

The dynamics of A3565 is significantly influenced by the presence of IC 4296, which, although not classified as a cD, does present an extended profile quantified by a value of  $n=11.8$  for a Sersic law (Graham et al. 1996). Such flat profiles were noted by those authors as being typical of Brightest Cluster Galaxies. The large extent of this galaxy was also noted by Saglia et al. (1993) who presented the velocity dispersion profile out to a distance of  $0.8 R_e$  which corresponds to  $45''$  or  $7.7 h^{-1} \text{ kpc}$ . The internal velocity dispersion profile of this galaxy is greater than  $200 \text{ kms}^{-1}$  and has a rather flat appearance, indicating the presence of a massive dark halo (Saglia et al. 1993).

The velocity histogram of group members (corrected to the Local Group Centroid) is shown in Figure 5 where the dashed line indicates the radial velocity of IC 4296 ( $v_o = 3593 \text{ kms}^{-1}$ ). This is almost identical to the value of the bi-weight estimate for the central location velocity of the cluster ( $3586 \text{ kms}^{-1}$ ). This result differs from the conclusion of Kemp (1994), who found that a difference of  $\sim 150 \text{ kms}^{-1}$  between IC 4296 and the group’s mean radial velocity, though the reason for this discrepancy is unclear. The projected separation of IC 4296 to the group’s centroid about  $0.14 h^{-1} \text{ Mpc}$ . In order to check whether this could be due to the presence of interlopers at large angular separations, we also determined the dynamical parameters in the case where only galaxies within a radius of  $\sim 0.5^\circ$  ( $0.31 h^{-1} \text{ Mpc}$ ) from IC 4296 were considered. This radius



excludes galaxies such as NGC 5193 and NGC 5193A which, as mentioned in the Introduction, have been assigned to another system by Abell et al. (1989) and Lauer et al. (1998). This smaller sample contains 21 galaxies, and reduces the projected separation between the group center and IC 4296 to  $0.07 h^{-1}$  Mpc, while the radial velocity difference is slightly larger, increasing from  $7 \text{ kms}^{-1}$  to  $39 \text{ kms}^{-1}$ , still within the measurement errors. The velocity dispersion for this smaller sample also changes slightly ( $234 \text{ kms}^{-1}$ ). The mass estimators are  $\sim 10\%$  smaller ( $M_{VT} = 2.6 \times 10^{13} M_{\odot}$ ;  $M_p = 3.0 \times 10^{13} M_{\odot}$ ), but still within the errors estimated from the larger sample, suggesting that the larger sample probably contains no interlopers.

The spatial segregation between galaxies presenting emission lines (crosses), comprising 34% of the sample (10 galaxies), from the 19 (66%) galaxies that only present absorption line spectra (open squares), can be seen in Figure 4. The latter tend to be found in the central regions of the cluster, while emission line galaxies are predominant in the outer regions, a feature which is common in rich clusters, but only recently shown to occur also in poor clusters (Zabludoff & Mulchaey 1998a; Mahdavi et al. 1999). The observed segregation may be quantified through  $R_h$  and  $R_p$  which for the absorption line galaxies are  $R_h = 0.28 \pm 0.02 h^{-1}$  Mpc, and  $R_p = 0.47 \pm 0.04 h^{-1}$  Mpc, while for the emission line systems these are  $R_h = 0.67 \pm 0.03 h^{-1}$  Mpc and  $R_p = 0.66 \pm 0.10 h^{-1}$  Mpc, which are a factor of  $\sim 2$  larger than for the absorption line systems. For the entire sample the values are  $R_h = 0.40 \pm 0.01 h^{-1}$  Mpc and  $R_p = 0.57 \pm 0.03 h^{-1}$  Mpc. By running a two-sample Kolmogorov-Smirnov test on the projected distances of galaxies from the cluster center we find that the probability of both samples being drawn from the same parent population is at the 4% level; a similar result (3.6%) is obtained from Monte-Carlo simulations where the galaxy distances from the cluster center were bootstrapped. On the other hand the cluster velocity dispersion measured using either type of galaxy is to all effects identical. For the 19 absorption line systems we find  $231 (+51, -32) \text{ kms}^{-1}$  using the classical estimator, and  $242 \pm 42 \text{ kms}^{-1}$  using the bi-weight ROSTAT estimator, while for the 10 emission line systems these are  $232 (+82, -41) \text{ kms}^{-1}$  and  $235 \pm 66$ , respectively. The values for both galaxy populations are very similar to the velocity dispersion of the entire sample  $228 (+38, -26) \text{ kms}^{-1}$  and  $236 \pm 69 \text{ kms}^{-1}$ .

The distribution of absolute magnitudes is presented in Figure 6, where galaxies are counted in 0.5 magnitude bins. The faintest absolute magnitude that can be reached with this sample is  $\sim 3$  magnitudes fainter than the value of  $M_R^*$  ( $-20.29 \pm 0.02 + 5 \log h$ , Lin et al. 1996). In the figure we may see a dip in the absolute magnitude distribution at  $M_R \sim -19$ . This is at a similar value to that found by Koranyi et al. (1998) in AWM 7 as well as in other systems, and which could be a common feature to rich clusters, due to a depletion of galaxies as a result of mergers (Koranyi et al. 1998). However, because of the small number of galaxies in A3565, we cannot consider this feature as being significant as it could be just a fluctuation due to small number statistics.

In the study of groups and poor clusters presenting diffuse X-ray emission detected by *ROSAT*, Mulchaey et al. (1996) present in their Figure 4 the X-ray contours overlaid on a Digital Sky Survey map covering a  $1^\circ \times 1^\circ$  region centered on IC 4296. There one can see that the X-ray emission is not centered on IC 4296, but presents a peak between IC 4296 and IC 4299, having a

rather irregular shape aligned NE-SW. By fitting a modified King model

$$S(r) = S_0\{1 + (r/R_{core})^2\}^{-3\beta+0.5} + B_0 \quad (1)$$

to the counts, Mulchaey et al. (1996) measured  $\beta = 0.46$  and a temperature  $T = 1.07$  keV. In their model, Mulchaey et al. (1996) considered the gas profile out to a maximum extent of 21.5 arc min or  $0.23 h^{-1}$  Mpc from IC 4296, where the gas reaches 20% of the background level. The mass estimated from the X-ray model is of the order of  $1.17 \times 10^{13} M_{\odot}$ , which is about a factor of 3 smaller than the mass we derive from the galaxy distribution. By extrapolating the model of Mulchaey et al. (1996) out to the value of the harmonic radius measured in this work we find that the mass estimate ( $1.57 \times 10^{13} M_{\odot}$ ) is still only about a half of the total mass obtained from the virial and projected mass estimators.

As noted above, IC 4296 has an internal velocity dispersion  $\sim 200 \text{ kms}^{-1}$ , which reaches up to  $\sim 300 \text{ kms}^{-1}$  in its central regions (Wegner et al. 1999; Kemp 1994). This value is comparable to the velocity dispersion of A3565, and it is interesting to note that of the sample of 12 clusters studied by Zabludoff & Mulchaey (1998a), only 2 present a similar feature, although the significance of this result is unclear. The high value of the velocity dispersion could imply that at least some of the X-ray emitting gas is more influenced by the galaxy rather than the cluster (e.g., David & Blumenthal 1992). The scenario where gas is bound by the central galaxy as well as by the cluster potential is consistent with the conclusions of Mulchaey & Zabludoff (1998a), who obtained better fits to the observed X-ray distribution when a two-component model was considered: one component would be due to the central galaxy and the second component due to the diffuse gas. Such a scenario was considered by Mulchaey et al. (1996), to explain the rather low value of  $\beta$  they measured for A3565.

### 3.3. A3560

In Figure 7 we show the distribution of galaxies with radial velocities between  $13000 \text{ kms}^{-1} \leq v_{\odot} \leq 16000 \text{ kms}^{-1}$ , which roughly corresponds to the redshift interval of the Shapley Concentration. In addition to A3560 there is a dispersed distribution of galaxies which belong to the Shapley Supercluster, but are not part of the cluster. Even though A3560 is close to the NW border of the surveyed region, enough galaxies are contained in the survey that an estimate of the dynamical parameters of the cluster is possible. In this analysis we will consider the galaxies within the range of  $13^h 28^m < \alpha < 13^h 33^m$  and  $-32^{\circ} 35' > \delta > -33^{\circ} 20''$  as likely members. Within these limits and the radial velocity range above, there are 33 galaxies. Their distribution seen in Figure 7 suggests that A3560 could be composed of two concentrations of galaxies. This is also suggested by the histogram of radial velocities in Figure 8, where two velocity peaks are seen: one at  $\sim 13600 \text{ kms}^{-1}$  and the other at  $\sim 14800 \text{ kms}^{-1}$ . In order to confirm whether both the spatial and redshift distribution could be due to subclustering, we applied the statistical tests described by Pinkney et al. (1996) to the sample. Only the Lee 2-D and Lee 3-D statistics detect any

significant level of subclustering. The Dressler & Shectman (1988)  $\Delta$  statistic in particular, which is the most sensitive test (Pinkney et al. 1996), detects no significant evidence of subclustering. Therefore, in the determination of the physical parameters for A3560, shown in the last column of Table 5, we will assume that there is no subclustering. In the analysis that follows we also applied the  $3\sigma$  clipping algorithm (Yahil & Vidal 1977), which removes one galaxy from the sample (WMMA 076,  $v_{\odot} = 13361 \text{ kms}^{-1}$ ).

The velocity dispersion we measure for this cluster, ( $588 \text{ kms}^{-1}$ ) is smaller than that measured by Melnick & Moles (1987),  $838 \text{ kms}^{-1}$  which was based on 10 galaxies. Our mass estimate using the Virial Theorem ( $\sim 2 \times 10^{14} M_{\odot}$ ) is close to the value estimated by Ettori et al. (1997) from X-ray data ( $\sim 2.3 \times 10^{14} M_{\odot}$ ). The projected mass is a factor of 2 larger than the Virial estimator, and this could be due to the combination of the small sample size with a somewhat complex distribution of galaxies, which is seen not only in the optical data, but also in the X-ray maps for this cluster of Pierre et al. (1994). As may be seen in their Figure 6, there are four X-ray peaks in the direction of A3560, and excepting for the most extended source, they are not well correlated with the distribution of galaxies down to the limiting magnitude used in this work.

We should note that the centroid we determine here for A3560 differs from the position of Melnick & Moles (1987), probably because of the larger range in right ascension we are considering. The range used here corresponds to  $\sim 1.6 h^{-1} \text{ Mpc}$  at the mean cluster distance. The centroid in Table 5 is about  $0.13^{\circ}$ , or  $0.32 h^{-1} \text{ Mpc}$  away from the position of galaxies WMMA 032 and WMMA 033 in Table 4, which form a dumbbell system (Gregorini et al. 1994). The fact that this type of system is typically found in the central regions of clusters (Valentijn & Casertano 1988), suggests that the centroid of A3560 may be close to this position. Further support for this interpretation is the presence of the main component of the diffuse X-ray emission detected by Pierre et al. (1994) which also peaks close to the position of the dumbbell galaxy. In particular, if one considers the sample of galaxies to  $R_F = 16.0 \text{ mag}$ , which has 80% radial velocity completeness, the distribution of galaxies with redshifts centered on the dumbbell becomes much more pronounced. Furthermore, the fact that the mass-to-light ratio is large ( $\sim 760 (M/L_R)_{\odot}$ ) is also suggestive that the cluster membership as considered in this work is uncertain. All these results suggest that our conclusions regarding A3560 should only be considered as preliminary, since a larger and fainter sample will be required to describe more accurately the distribution of galaxies in this region.

The radial velocities of the dumbbell components differ by  $10 \text{ kms}^{-1}$ , while their projected separation is of the order of  $9 h^{-1} \text{ kpc}$ . Both values are somewhat smaller than the typical values for this kind of system quoted by Valentijn & Casertano (1988). Both nuclei have absorption line spectra, neither presenting any significant evidence of having undergone recent episodes of star formation. The mean radial velocity of these systems is shown in Figure 8 as a dotted line, which is about  $60 \text{ kms}^{-1}$  away from the mean radial velocity of the group in Table 5.

## 4. Conclusions

In this paper we have presented the redshift survey of a  $2.17^\circ \times 2.17^\circ$  region centered on the galaxy IC 4296, which is the brightest galaxy in the A3565 cluster. The present work extends the coverage of galaxies of A3565 to a limit of  $M_R^* + 3$ , within a radius of  $\sim 0.7 h^{-1}$  Mpc. Both the radial extent and the number of members for this cluster are comparable to what was found for similar systems by Zabludoff & Mulchaey (1998a) and Mulchaey & Zabludoff (1998a) in their study of the optical and X-ray properties of 12 poor clusters of galaxies. The velocity dispersion, as well as the mass we measure for A3565 are within the range of values quoted in those works, and A3565 has dynamical properties typical of X-ray emitting poor clusters.

This cluster contains galaxies undergoing interactions (NGC 5215A and NGC 5215B; Kemp & Meaburn 1991), and with common haloes (IC 4296 and IC 4299; Kemp 1994). This evidence coupled to the small value of the velocity dispersion of the system suggests that bright galaxies could still be forming in A3565 through mergers. Such a scenario has been suggested in recent works by Mulchaey & Zabludoff (1998b) and Zabludoff & Mulchaey (1998b) who find that the brightest galaxies in groups as well as the groups themselves could still be forming through the accretion of smaller systems, and that the merger rate is most efficient in groups with  $\sigma \sim 200$   $\text{kms}^{-1}$ , which is the case of A3565.

As in other poor clusters with diffuse X-ray emission, (e.g., Zabludoff & Mulchaey 1998a; Mahdavi et al. 1999), A3565 also shows radial segregation between galaxies presenting emission lines, mainly found in the outer parts of the cluster, while absorption line systems are concentrated towards the cluster center. This radial segregation together with the bending of the radio jets of IC 4296 noted by Killeen & Bicknell (1988), and the presence of several galaxies with distorted morphologies (Kemp & Meaburn 1993), suggest that the Intergalactic Medium of A3565 could also play an important role in the dynamical evolution of this system.

We also measured redshifts of galaxies belonging to the A3560 cluster, a background system that belongs to the Shapley Concentration. Although the velocity dispersion we measure for A3560 ( $\sim 580$   $\text{kms}^{-1}$ ) is typical of rich galaxy clusters, our results for this cluster should only be taken as preliminary. This is suggested by the relatively bright limiting absolute magnitude of our work at the distance of A3560 ( $M_{lim} \sim M_R^*$ ); the relatively complex distribution of galaxies and X-ray emission; the discrepancies between the mass estimators, and the large M/L ratio we measure. Therefore, to characterize the membership and dynamics of this cluster, a larger and fainter sample will be needed.

### A. Additional Galaxies

A more extensive though shallower survey in a larger ( $5^\circ \times 5^\circ$ ) region in the general direction of A3565 shows no significant increase in the number of cluster members. A further 51 galaxies

were observed, and are listed in Table 6 where column (1) shows the HSTGC identification, and in column (2) other identifications if known; columns (3) and (4) the right ascension and declination for epoch B1950.0 followed by the new radial velocity and the internal estimated error, respectively in columns (5) and (6). In this table we also include three serendipitous objects that were observed in the course of the survey, which are noted in the table. The coordinates for these three objects were estimated from the DSS. Because most objects in Table 6 were defined from a blue selected sample with  $m_B \leq 15.5 \text{ mag}$ , where  $m_B$  is the blue magnitude at the  $26 \text{ mag arcsec}^{-2}$  (Alonso et al. 1993; da Costa et al. 1998), we did not include them in the analysis of the group. However, the distribution of galaxies may be seen in Figure 9, where we code galaxies in different redshift intervals as in Figure 4. The main feature to note is that very few galaxies in the redshift interval of A3565 are added in the outskirts of the cluster.

We would like to thank Marcelo Assafin for his help on the astrometric calibration, Jason Pinkney for providing the code to calculate significance levels of subclustering, and Ricardo Schiavon for the observations in the s11 run. We also thank Ann Zabludoff, David Buote, George Blumenthal and Hernán Muriel for useful conversations. Financial support for this work has been given through FAPERJ (CNAW, MAGM, OLC, DFM), CNPq grants 301364/86-9 (CNAW), 301366/86-1 (MAGM), 301456/95 (DFM); NSF AST 9529098 (CNAW); and PICT97 No. 03-00000-01213 (FONCyT), CONICOR, SECyT, and CONICET (MVA) and Fundación Antorchas–Vitae–Andes cooperation. LAR and SOM were supported by CNPq undergraduate studentships offered by the CNPq/ON through the PIBIC program. This research has made use of the NASA/IPAC Extragalactic Database (NED) which is operated by the Jet Propulsion Laboratory, CALTECH, under contract with the National Aeronautics and Space Administration. We acknowledge the use of NASA’s *SkyView* facility (<http://skyview.gsfc.nasa.gov>) located at NASA Goddard Space Flight Center, and the use of the CCD and data acquisition system supported under U.S. National Science Foundation grant AST-90-15827 to R.M. Rich. We acknowledge use of the Digitized Sky Survey, produced at the Space Telescope Science Institute under U.S. Government grant NAG W-2166. The images are based on photographic data obtained using UK Schmidt Telescope, operated by the Royal Observatory Edinburgh, with funding from the UK Science and Engineering Research Council (later the UK Particle Physics and Astronomy Research Council), until 1988 June, and thereafter by the Anglo-Australian Observatory.

## REFERENCES

- Abell, G. O., Corwin, H.G., & Olowin, R.P. 1989, *ApJS*, 70, 1
- Alonso, M. V., da Costa, L. N., Pellegrini, P. S. & Kurtz, M. J. 1993, *AJ* 106, 676
- Arp H. C., & Madore, B. F. 1987, “A Catalogue of Southern Peculiar Galaxies and Associations”, (Cambridge: Cambridge Univ. Press) (AM)
- Assafin, M., , Martins, R. Vieira, & Andrei, A. H. 1997, *AJ*, 113, 1451

- Bardelli, S., Pisani, A., Ramella, M., Zucca, E., & Zamorani, G. 1998, MNRAS 300, 589
- Beers, T. C., Flynn, K. & Gebhardt, K. 1990, AJ, 100, 32
- Bothun, G., Geller, M. J., Beers, T. C. & Huchra, J. P. 1983, ApJ 268, 47
- Brown, D., L., & Burns, J. O. 1991, AJ, 102, 1917
- Buote, D. A., & Fabian, A. C., 1998, MNRAS, 296, 977
- Buta, R. 1995, ApJS, 96, 39 (CSRG)
- Corbin, T. & Urban, S. 1988, in I.A.U. Symp. No. 133, “Mapping the Sky”, ed. H. Eichhorn (Dordrecht: Reidel), 75
- Coté, S., Freeman, K. C., Carignan, C., & Quinn, P. J. 1997, AJ, 114, 1313
- da Costa, L.N., Pellegrini, P.S., Nunes, M.A., Willmer, C., Chincarini, G., & Cowan, J. 1986, AJ, 91, 6 (DC1)
- da Costa, L.N., Pellegrini, P. S., Willmer, C., de Carvalho, R., Maia, M., Latham, D. W. & Geary, J. C. 1989, AJ, 97, 315
- da Costa, L.N., Willmer, C. N. A., Pellegrini, P.S., Chaves, O. L., Rit e, C., Maia, M. A. G., Geller, M. J., Latham, D. W., Kurtz, M. J., Huchra, J. P., Ramella, M., Fairall, A. P., Smith, C., & L ipari, S. 1998, AJ, 116, 1
- da Costa, L.N., Willmer, C., Pellegrini, P.S., & Chincarini, G. 1987, AJ, 93, 1338 (DC2)
- David, L. P., & Blumenthal, G. R. 1992, ApJ 389, 510
- Danese, L., De Zotti, G., & di Tullio, G. 1980, A&A, 82, 322
- Dressler, A., & Shectman, S. A. 1988, AJ, 95, 985
- Drinkwater, M. J., Proust, D., Parker, Q. A., Quintana, H., & Slezak, E. 1999, PASAu, in press; astro-ph/9903028
- Ebeling, H., Voges, W., B ohringer, H., Edge, A. C., Huchra, J. P. & Briel, U. G. 1996, MNRAS, 281, 799
- Ettori, S., Fabian, A. C., & White, D. A. 1997, MNRAS, 289, 787
- Forman, W., Jones, C., & Tucker, W. 1985, ApJ, 293, 102
- Garcia, A. M. 1993, A&AS, 100, 47
- Graham, A. W., Lauer, T. D., Colless, M. & Postman, M. 1996, ApJ 465, 534
- Gregorini, L., de Ruiter, H. R., Parma, P., Sadler, E. M., Vettolani, G., & Ekers, R. D. 1994, A&AS, 106, 1
- Heisler, J., Tremaine, S., & Bahcall, J. N. 1985, ApJ, 298, 8
- Huchra, J. P., & Geller, M. G. 1982, ApJ, 257, 243
- Jarvis, J.F., & Tyson, J.A. 1981, AJ, 86, 476

- Jørgensen, I., Franx, M., & Kjaergaard, P. 1995, MNRAS 276, 1341
- Kemp, S. N. 1994, A&A, 282, 425
- Kemp, S. N., & Meaburn, J. 1991, MNRAS, 252, 27
- Kemp, S. N., & Meaburn, J. 1993, A&A, 274, 19
- Killeen, N. E. B., & Bicknell, G. V. 1988, ApJ, 324, 198
- Koranyi, D. M., Geller, M. J., Mohr, J. J., & Wegner, G. 1998, AJ, 116, 2108
- Kurtz, M. J. & Mink, D. J. 1998, PASP, 110, 934
- Kurtz, M. J., Mink, D. J., Wyatt, W. F., Fabricant, D. G., Torres, G., Kriss, G. A., & Tonry, J. L. 1992, in ASP Conf. Ser. Vol. 25, Proc. 1<sup>st</sup> Ann. Conf. Astronomical Data Analysis Software and Systems, ed., D.M. Worrall, C. Biemesderfer, & J. Barnes (San Francisco: ASP), 432
- Lasker, B.M., Sturch, C.R., McLean, B.M., Russel, J.L., Jenker, H., & Shara, M. 1990, AJ, 99, 2019 (HSTGC)
- Lauberts, A., & Valentijn, E.A. 1989, The Surface Photometry Catalogue of the ESO-Uppsala Galaxies, (Garching: ESO) (ESO-LV)
- Lauer, T. R. & Postman, M. 1994, ApJ, 425, L418
- Lauer, T. R., Tonry, J. L., Postman, M., Ajhar, E. A. & Holtzman, J. A. 1998, ApJ 499, 577
- Lin, H., Kirshner, R. P., Schectman, S. A., Landy, S. D., Oemler, A., Tucker, D. L. & Schechter, P. L. 1996, ApJ, 471, 617
- Lynden-Bell, D., Faber, S.M., Burstein, D., Davies, R.L., Dressler, A., Terlevich, R.J., & Wegner, G. 1988, ApJ, 326, 19
- Lynden-Bell, D., Lahav, O., & Burstein, D. 1989, MNRAS, 241, 325
- Maia, M.A.G., da Costa, L.N., & Latham, D.W. 1989, ApJS, 69, 809
- Massey, P. 1992, A User's Guide to CCD Reductions with IRAF (Tucson: KPNO Computer Support Group)
- Maddox, S. J., Efstathiou, G. & Sutherland, W. J. 1990, MNRAS 246, 433
- Mahdavi, A., Geller, M. J., Boehringer, H., Kurtz, M. J. & Ramella, M. 1999, astro-ph/9901095
- Marston, A. P. 1988, MNRAS, 230, 97
- Matthewson, D. S., Ford, V. L. & Buckhorn, M. 1992, ApJS, 81, 413
- Melnick, J. & Moles, M. 1987, RMxAA, 14, 72
- Metcalfe, N., Godwin, J. G., & Peach, J. V. 1994, MNRAS, 267, 431
- Mills, B. Y., Slee, O. B., Hill, E. R. 1960, Aust.J. Phys. 13, 676
- Mount Stromlo Abell Cluster Supernova Search Team, 1997, IAU Circular 6708A

- Mould, J. R., Staveley-Smith, L., Schommer, R. A., Bothun, G. D., Hall, P. J., Han, M. S., Huchra, J. P., Roth, J., Walsh, W., & Wright, A. E. 1991, *ApJ*, 383, 467
- Mulchaey, J. S., Davis, D. S., Mushotzky, R. F., & Burstein, D. 1996, *ApJ*, 456, 80
- Mulchaey J. S., & Zabludoff, A., I. 1998a, *ApJ*, 496, 73
- Mulchaey J. S., & Zabludoff, A., I. 1998b, *astro-ph/9810458*
- Nolthenius, R. 1993, *ApJS*, 85, 1
- Paturel, G., Petit, C., Kogoshvili, N., Dubois, P., Bottinelli, L., Fouque, P., Garnier, R. & Gouguenheim, P. 1991, *A&AS*, 91, 371
- Pierre, M., Böhringer, H., Ebeling, W., Vosges, W., Schuecker, P., Crudacce, R., & MacGillivray, H. 1994, *A&A*, 290, 725
- Pinkney, J., Roettinger, K, Burns, J. O., & Bird, C. M. 1996, *ApJS* 104, 1
- Postman, M. & Lauer, T. R., 1995, *ApJ*, 440, 28
- Quintana, H., Ramirez, A., Melnick, J., Raychaudhury, S., & Slezak, E. 1995 *AJ* 110, 463 (QRM)
- Ramella, M., et al. 1999, *A&A*, 342, 1
- Ramella, M., Geller, M. J., & Huchra, J. P. 1989, *ApJ*, 344, 57
- Richter, O. -G. 1984, *A&AS*, 58, 131
- Richter, O. -G. 1987, *A&AS*, 67, 261
- Röser, S., & Bastian, U. 1991, *PPM Star Catalogue* (Heidelberg: Spektrum Akademischer Verlag)
- Saglia, R. P., Bertin, G., Bertola, F. Danziger, J., Dejonghe, H., Sadler, E. M., Stiavelli, M., de Zeeuw, P. T., Zeilinger, W. W. 1993, *ApJ* 403, 567
- Sandage, A. 1972, *ApJ*, 178, 1
- Schlegel, D. J., Finkbeiner, D. P. & Davis, M., 1998, *ApJ*, 500, 525
- Theureau, 1998, *A&AS*, 130, 333 (T98)
- Valdes, F. 1982, *Focas User's Manual* (2<sup>nd</sup> ed.; Tucson: KPNO Computer Support Group)
- Valentijn, E. A., & Casertano, S. 1988, *A&A* 206, 27
- Vettolani, G., Chincarini, G., Scaramella, R. & Zamorani, G. 1990, *AJ*, 99, 1709
- Wegner, G. et al. 1999, *in preparation*.
- West, M. J., Oemler, A., & Dekel, A. 1988, *ApJ*, 327, 1
- Willmer, C.N.A., Focardi, P., Chan, R., Pellegrini, P.S., & da Costa, L.N. 1991, *AJ* 101, 57
- Yahil, A., Vidal, N. V. 1977, *ApJ*, 214, 347
- Zabludoff, A., I., & Mulchaey, J., S. 1998a, *ApJ*, 496, 39
- Zabludoff, A., I., & Mulchaey, J., S. 1998b, *ApJ*, 498, 5



Table 1. Observations: Photometry

code	date	telescope	CCD	Format	Scale ["/pix]	Gain [e <sup>-</sup> /ADU]	RON [e <sup>-</sup> ]
(1)	(2)	(3)	(4)	(5)	(6)	(7)	(8)
<i>p1</i>	1996 March 21	0.60 m	LNA#301	578 × 385	1.13	2.63	5.4
<i>p2</i>	1997 May 2	1.60 m	LNA#48	770 × 1152	0.57	5.59	10.67

Table 2. Galaxies in Scans with CCD Photometry

WMMA Id. (1)	Identification (2)	$R_{24}$ (3)	$R_{25}$ (4)	$R_{26}$ (5)	Run (6)
008	NGC 5193A, 383 G 14	12.98 ± 0.22	13.05 ± 0.18	13.11 ± 0.13	p1
011	NGC 5193, 383 G 15	11.27 ± 0.17	11.17 ± 0.31	11.14 ± 0.40	p1
125		16.15 ± 0.05	16.06 ± 0.06	15.98 ± 0.08	p1
126	383G37	13.24 ± 0.05	13.16 ± 0.06	13.11 ± 0.07	p1
135	B133341.2-334911	14.01 ± 0.05	13.97 ± 0.05	13.93 ± 0.06	p1
137	IC 4296, 383 G 39	10.24 ± 0.05	10.08 ± 0.06	9.93 ± 0.06	p1
141	IC 4299, 383 G 42	12.18 ± 0.05	12.16 ± 0.05	12.13 ± 0.05	p1
159	383 G 45	12.48 ± 0.05	12.43 ± 0.05	12.38 ± 0.05	p1
171	383 G 49	13.11 ± 0.06	12.84 ± 0.06	12.57 ± 0.06	p2
192	383 G 55	14.40 ± 0.06	14.22 ± 0.06	14.03 ± 0.06	p2
204		15.89 ± 0.06	15.74 ± 0.06	15.58 ± 0.06	p2
206	B133737.8-334408	16.09 ± 0.06	15.94 ± 0.06	15.83 ± 0.06	p2
208		15.32 ± 0.06	15.02 ± 0.06	14.71 ± 0.06	p2
209		14.53 ± 0.06	14.32 ± 0.06	14.11 ± 0.06	p2
231		14.68 ± 0.05	14.49 ± 0.05	14.31 ± 0.05	p2

Table 3. Observations: Spectroscopy

code	date	telescope	CCD	Format	Grating [1/mm]	Dispersion [Å/pix]	Resolution [Å]	$\lambda$ coverage [Å]
(1)	(2)	(3)	(4)	(5)	(6)	(7)	(8)	(9)
s1	1994 May	CASLEO 2.15m	EEV P8603S	385 × 578	600	2.4	7.3	4650–6050
s2	1994 Jul	CASLEO 2.15m	EEV P8603S	385 × 578	300	4.7	14.0	4100–6800
s3	1995 Mar	OPD 1.60m	EEV P8603A	1156 × 770	900	1.2	3.1	4770–6135
s4	1995 Apr	CASLEO 2.15m	Tek	1024 × 1024	600	1.6	5.0	5100–6800
s5	1997 Jan	ESO 1.52m	Loral	2048 × 2048	600	1.7	4.3	3600–7500
s6	1997 Apr/May	ESO 1.52m	Loral	2048 × 2048	600	1.7	4.3	3600–7500
s7	1997 Jun	ESO 1.52m	Loral	2048 × 2048	600	1.7	4.3	3600–7500
s8	1998 Feb/Mar	ESO 1.52m	Loral	2048 × 2048	600	1.7	4.3	3600–7500
s9	1998 Apr	ESO 1.52m	Loral	2048 × 2048	600	1.7	4.3	3600–7500
s10	1998 Jun	ESO 1.52m	Loral	2048 × 2048	600	1.7	4.3	3600–7500
s11	1999 Feb	ESO 1.52m	Loral	2048 × 2048	600	1.7	4.3	3550–7450

Table 4. Galaxies in the Scanned Region

WMMA Id.	Identification	R.A.	Dec.	$R_F$	T	$v_{\odot}$	$\pm$	$N_e$	Ref
(1)	(2)	B1950.0	B1950.0	(5)	(6)	$\text{kms}^{-1}$	$\text{kms}^{-1}$	(9)	(10)
		(3)	(4)			(7)	(8)		
001	NGC 5188, 383 G 09	13:28:39.6	-34:32:19	11.03	5	2425	6	0	T98
002		13:28:40.4	-34:15:48	15.84	5	-	-	-	-
003		13:28:47.6	-34:06:48	15.49	5	13798	40	3	s11
004		13:28:49.6	-32:59:09	14.43	5	16554	40	0	s2
005	383 G 12	13:28:53.1	-33:07:23	13.89	5	7759	21	1	s9
006		13:28:53.1	-32:56:21	15.84	-5	15449	35	0	s8
007		13:28:56.4	-32:38:12	14.10	-2	14780	46	0	s9
008	NGC 5193A, 383 G 14	13:28:58.9	-32:58:52	13.30	-2	3519	21	0	s6
009	GDP 1 <sup>a</sup>	13:29:01.2	-32:56:18	15.35	-5	14852	40	0	s8
010		13:29:02.0	-33:23:48	16.13	-2	-	-	-	-
011	NGC 5193, 383 G 15	13:29:03.1	-32:58:39	11.69	-5	3745	20	0	s8
012		13:29:08.9	-33:47:07	15.45	5	14246	49	4	s10
013		13:29:09.0	-33:47:45	16.28	5	-	-	-	-
014		13:29:09.6	-32:50:12	16.09	5	-	-	-	-
015		13:29:10.9	-32:38:20	16.28	5	-	-	-	-
016		13:29:12.8	-32:48:34	15.60	-2	-	-	-	-
017		13:29:13.1	-32:37:29	15.27	5	14033	28	0	s10
018	B132914.5-333157 <sup>b</sup>	13:29:14.4	-33:31:58	15.39	5	8755	25	4	s5
019	B132916.4-330338 <sup>b</sup>	13:29:16.5	-33:03:41	15.06	-5	13820	33	4	s5
020		13:29:17.4	-32:45:13	14.65	-2	14807	38	0	s2
021		13:29:18.8	-33:07:46	15.51	-2	-	-	-	-
022		13:29:19.0	-33:03:32	15.46	5	7539	58	8	s5
023	AM 1329-324 <sup>c</sup>	13:29:19.6	-32:40:35	15.09	-5	14214	106	0	QRM
024		13:29:19.7	-34:06:19	16.35	5	-	-	-	-
025		13:29:19.9	-33:20:32	16.17	-2	-	-	-	-
026	AM 1329-324 <sup>c</sup>	13:29:19.9	-32:40:22	15.09	-2	14801	49	0	s10
027		13:29:22.4	-32:52:14	15.54	-2	14541	30	0	s11
028	B132924.5-330715 <sup>b</sup>	13:29:24.6	-33:07:15	14.76	5	15292	43	0	s2
243		13:29:27.5	-32:53:17	16.64	-2	13502	51	0	s11
029		13:29:28.6	-32:39:48	15.20	-2	15703	29	0	s5
030	HSTGC 07269-01549 <sup>d</sup>	13:29:29.7	-32:53:45	15.19	-2	14868	26	0	s10
031	QRM 1325-32 41 <sup>e</sup> B132933.4-325855 <sup>b</sup>	13:29:33.4	-32:58:55	14.89	-2	13880	39	0	s5
032	QRM 1325-32 37 <sup>e</sup>	13:29:34.5	-32:52:53	15.29	16	14734	32	0	s11
033	QRM 1325-32 38 <sup>e</sup>	13:29:35.3	-32:52:44	14.44	16	14724	25	0	s11
034		13:29:37.0	-32:50:50	15.80	5	-	-	-	-
035		13:29:39.1	-32:59:35	14.93	5	14592	51	0	s7
036	QRM 1325-32 42 <sup>e</sup>	13:29:40.1	-32:54:20	15.72	-2	14595	46	0	QRM
037		13:29:41.0	-32:54:55	16.15	-2	-	-	-	-
038	QRM 1325-32 40 <sup>e</sup>	13:29:43.1	-32:53:53	14.72	-5	12516	26	0	QRM
039		13:29:44.0	-33:02:47	16.05	5	-	-	-	-
040	AM 1329-325 <sup>c</sup>	13:29:46.2	-32:51:30	15.09	-2	15410	29	0	s5
041	AM 1329-325 <sup>c</sup>	13:29:46.3	-32:51:30	14.94	-2	15031	48	0	s5
042		13:29:50.9	-34:38:31	16.29	5	-	-	-	-
043		13:29:54.5	-32:58:58	15.33	5	14222	32	0	s10
044		13:29:55.6	-33:08:46	15.84	5	-	-	-	-
045		13:29:59.8	-32:46:43	15.01	16	13410	26	6	s8
046	B133000.5-342742 <sup>b</sup>	13:30:00.4	-34:27:42	15.67	5	36879	77	0	DPP
047		13:30:00.7	-32:46:20	15.89	5	13451	51	2	s8
048		13:30:02.3	-34:43:34	16.00	5	-	-	-	-
049		13:30:02.8	-34:26:34	16.32	5	-	-	-	-
050		13:30:03.8	-33:03:46	16.31	5	-	-	-	-
051	QRM 1330-32 04 <sup>e</sup> B133004.4-325449 <sup>b</sup>	13:30:04.3	-32:54:50	15.04	-2	15749	26	0	s5
052		13:30:05.9	-33:07:02	16.09	5	-	-	-	-
053		13:30:07.9	-32:51:31	15.66	5	15127	30	0	s8
054		13:30:09.6	-32:49:32	15.95	5	-	-	-	-
055	B133010.9-325038 <sup>b</sup>	13:30:11.3	-32:50:38	14.50	-2	15006	25	0	s8
056		13:30:11.7	-34:02:28	15.08	5	14435	37	3	s5
057	QRM 1330-32 08 <sup>e</sup>	13:30:13.0	-32:57:32	14.88	5	13732	40	0	s5
058		13:30:13.6	-32:54:47	16.10	5	-	-	-	-
059	B133014.9-330241 <sup>b</sup>	13:30:14.9	-33:02:41	15.53	5	14838	115	0	DPP
060	B133015.5-341136 <sup>b</sup>	13:30:15.5	-34:11:36	15.04	5	7451	38	6	s5
061		13:30:24.7	-32:57:45	16.25	-2	-	-	-	-
241	383 G 17	13:30:25.1	-34:12:38	15.70	22	3471	10	0	CFCQ
062		13:30:30.3	-33:41:15	15.70	5	-	-	-	-
063		13:30:31.0	-32:49:35	15.33	5	14490	33	0	s10
064		13:30:32.0	-32:59:34	15.90	-2	-	-	-	-
065	B133034.1-334134 <sup>b</sup>	13:30:34.0	-33:41:35	16.28	5	22010	143	0	DPP
066		13:30:34.5	-33:40:49	15.66	5	-	-	-	-

Table 4—Continued

WMMA Id.	Identification	R.A.	Dec.	$R_F$	T	$v_{\odot}$	$\pm$	$N_e$	Ref
(1)	(2)	B1950.0	B1950.0	(5)	(6)	$\text{kms}^{-1}$	$\text{kms}^{-1}$	(9)	(10)
		(3)	(4)			(7)	(8)		
067	383 G 18	13:30:34.7	-33:45:33	14.72	5	3721	17	3	s1
068		13:30:45.8	-32:57:04	15.68	5	-	-	-	-
069		13:30:51.9	-33:08:41	15.90	5	-	-	-	-
070		13:30:55.0	-32:54:46	15.10	5	15355	27	0	s10
071		13:30:55.9	-32:57:00	16.12	5	14957	37	0	s11
072		13:30:56.0	-32:54:34	15.10	33	-	-	-	-
073		13:30:57.9	-32:58:06	15.94	33	-	-	-	-
074		13:30:58.8	-33:21:14	16.22	5	-	-	-	-
075		13:31:00.5	-33:03:53	15.15	5	14595	78	0	s1
076		13:31:02.0	-32:45:29	14.39	-2	13361	45	0	s1
077		13:31:02.8	-33:06:25	15.26	5	14999	41	0	s5
078		13:31:03.3	-34:38:53	15.24	5	8177	83	7	s5
079		13:31:09.2	-33:32:19	16.07	5	-	-	-	-
080		13:31:13.4	-33:15:07	16.04	5	-	-	-	-
081		13:31:17.1	-32:59:53	15.25	5	13762	55	5	s10
082		13:31:20.4	-33:16:13	15.30	5	14031	23	5	s10
083	383 G 22, B133121.8-324317 <sup>b</sup>	13:31:21.9	-32:43:17	14.38	0	15207	35	0	s1
084		13:31:26.9	-33:48:54	13.97	5	3692	29	0	s3
085		13:31:30.4	-32:58:21	16.10	5	-	-	-	-
086		13:31:31.6	-33:42:35	16.28	5	-	-	-	-
087		13:31:35.9	-34:25:02	15.22	5	14848	49	0	s10
088		13:31:39.9	-32:43:02	15.48	-2	14946	34	0	s11
089		13:31:46.6	-32:51:59	15.61	5	-	-	-	-
090		13:31:48.0	-33:12:07	14.47	5	13866	40	2	s2
091	B133148.9-344649 <sup>b</sup>	13:31:48.6	-34:46:43	15.70	5	2367	21	0	DPP
092	383 G 24	13:31:50.1	-33:15:48	15.08	5	3270	79	8	s8
093		13:31:50.2	-33:46:55	16.21	5	-	-	-	-
094	MCG-06-30-010, 383 G 25	13:31:54.3	-34:03:17	13.22	0	3994	35	1	s1
095		13:31:56.7	-33:19:40	16.14	5	-	-	-	-
096		13:31:57.0	-32:53:30	14.51	5	15452	36	2	s5
097		13:31:57.9	-33:10:44	16.12	5	-	-	-	-
098		13:31:58.7	-32:49:24	15.34	5	15149	30	0	s10
099	CSRG 0728 <sup>f</sup>	13:32:02.3	-33:37:20	14.28	0	3809	71	0	s1
100		13:32:02.5	-32:46:53	16.00	5	-	-	-	-
101		13:32:04.3	-33:49:39	15.84	5	-	-	-	-
102		13:32:05.8	-33:57:39	15.56	5	-	-	-	-
103		13:32:08.3	-33:40:36	15.47	5	3949	65	0	s5
104	NGC 5215A, 383 G 29A	13:32:15.9	-33:13:29	13.27	16	3838	27	0	DC1
105		13:32:16.1	-34:01:46	15.71	5	-	-	-	-
106		13:32:16.8	-34:46:55	15.97	5	-	-	-	-
107		13:32:17.0	-34:02:01	15.71	16	-	-	-	-
108	B133217.4-334646 <sup>b</sup>	13:32:17.1	-33:46:46	14.69	5	3950	40	0	s8
109	NGC 5215B, 383 G 29	13:32:18.6	-33:13:39	12.86	16	4013	25	0	DC1
111		13:32:25.3	-33:49:19	15.06	5	13378	53	5	s8
112	MCG-05-32-043, 383 G 30	13:32:25.9	-33:38:34	12.91	5	3617	34	5	s11
113	MCG-06-30-013, 383 G 31	13:32:29.8	-33:57:02	12.85	5	7130	15	2	DC3
114	383 G 32, B133231.3-335420 <sup>b</sup>	13:32:31.3	-33:54:20	13.79	5	7465	93	0	s2
115		13:32:33.5	-33:37:54	16.36	5	-	-	-	-
116	MCG-06-30-014, 383 G 33	13:32:34.6	-33:56:06	14.49	5	7271	34	8	s5
117		13:32:35.9	-33:17:34	15.48	5	14294	29	0	s11
118		13:32:40.0	-33:58:27	15.97	5	-	-	-	-
119		13:32:44.0	-34:15:33	15.66	5	-	-	-	-
245		13:32:45.0	-33:15:52	16.64	5	7561	41	3	s11
120		13:32:49.9	-32:39:12	15.77	5	-	-	-	-
121		13:32:58.0	-33:59:14	14.77	5	3309	30	0	s8
122		13:33:01.9	-34:23:56	15.71	5	-	-	-	-
123	MCG-06-30-015, 383 G 35	13:33:01.9	-34:02:26	12.69	5	2358	19	3	s6
124	NGC 5220, 383 G 36	13:33:05.6	-33:11:51	12.06	-2	4213	20	0	s6
125		13:33:10.5	-32:45:08	15.95	5	-	-	-	-
126	MCG-05-32-048, 383 G 37	13:33:14.3	-32:45:21	13.23	5	3563	31	3	DC2
127		13:33:19.6	-33:38:22	15.37	-2	3542	43	0	s10
128		13:33:21.9	-34:07:11	15.13	5	3829	30	0	s10
129		13:33:23.1	-33:15:47	16.11	5	-	-	-	-
130		13:33:24.2	-33:21:49	14.74	5	3406	78	0	s8
131	383 G 38	13:33:27.3	-32:58:17	13.64	5	7507	50	0	s1
132		13:33:34.8	-34:00:56	15.53	5	-	-	-	-
133		13:33:36.7	-33:25:36	16.34	5	-	-	-	-
134	B133337.8-325015 <sup>b</sup>	13:33:37.8	-32:50:16	15.53	5	15688	105	0	DPP

Table 4—Continued

WMMA Id.	Identification	R.A.	Dec.	$R_F$	T	$v_{\odot}$	$\pm$	$N_e$	Ref
(1)	(2)	B1950.0 (3)	B1950.0 (4)	(5)	(6)	$\text{kms}^{-1}$ (7)	$\text{kms}^{-1}$ (8)	(9)	(10)
135	B133341.2-334911 <sup>b</sup>	13:33:41.1	-33:49:11	13.85	5	3850	20	2	s8
136		13:33:44.9	-33:39:30	16.34	-2	-	-	-	-
137	IC 4296, 383 G 39	13:33:47.1	-33:42:40	10.33	-5	3785	19	0	s6
138		13:33:47.5	-33:51:02	16.02	5	-	-	-	-
139		13:33:50.5	-32:53:34	15.49	33	7166	34	8	s11
140		13:33:52.6	-34:00:24	16.34	5	-	-	-	-
141	IC 4299, 383 G 42	13:33:55.6	-33:48:41	11.99	5	4045	52	0	s1
142		13:33:56.4	-33:28:30	16.18	5	-	-	-	-
143		13:34:02.7	-33:32:33	15.88	5	-	-	-	-
144	B133405.6-340842 <sup>b</sup>	13:34:05.6	-34:08:43	15.29	5	4109	23	4	s10
145	AM 1334-333 <sup>c</sup>	13:34:06.2	-33:29:49	13.78	5	11567	24	0	s6
146		13:34:06.8	-33:34:15	16.31	5	-	-	-	-
147	AM 1334-333 <sup>c</sup>	13:34:07.1	-33:29:27	14.90	5	4099	47	0	s6
148		13:34:09.4	-33:55:01	15.01	5	21348	35	0	s8
149	CSRG 0731 <sup>f</sup> B133411.1-333408 <sup>b</sup>	13:34:10.9	-33:34:04	14.07	5	14091	35	2	s6
150		13:34:17.0	-33:30:29	15.71	5	-	-	-	-
151	J133709.39-334731.9 <sup>g</sup>	13:34:17.0	-33:32:16	16.35	5	-	-	-	-
152	B133428.4-343809 <sup>b</sup>	13:34:28.3	-34:38:06	15.83	5	29247	103	0	DPP
153		13:34:29.1	-33:29:07	16.10	-2	-	-	-	-
154	MCG-05-32-052, 383 G 44	13:34:36.6	-32:45:10	13.29	5	3776	16	3	s3
155		13:34:38.4	-33:13:23	15.41	5	11275	26	8	s10
156		13:34:39.8	-34:24:18	15.20	5	17560	38	6	s10
157		13:34:42.4	-34:01:31	16.30	5	-	-	-	-
158	B133445.1-341642 <sup>b</sup>	13:34:45.1	-34:16:42	15.74	-2	22108	68	0	DPP
159	MCG-05-32-053, 383 G 45	13:34:47.6	-33:33:22	12.56	-2	3914	19	0	s6
160	B133449.6-333555 <sup>b</sup>	13:34:49.7	-33:35:53	15.19	5	11292	62	4	s8
161		13:34:55.0	-32:39:20	15.10	5	7447	24	0	s10
162	383 G 46	13:34:55.3	-34:33:14	15.04	5	13014	57	5	s5
163		13:34:55.9	-34:14:19	16.28	5	-	-	-	-
164		13:34:57.3	-33:34:25	16.08	5	-	-	-	-
165		13:35:01.1	-33:33:21	14.15	5	11402	28	0	s7
166		13:35:02.0	-34:28:10	16.17	5	-	-	-	-
167		13:35:08.7	-33:43:59	15.82	-2	37229	51	0	s8
168		13:35:08.8	-33:44:19	14.66	5	3698	29	0	s8
169	MCG-05-32-054, 383 G 48	13:35:09.5	-33:15:52	13.28	5	3702	25	3	s4
170		13:35:11.7	-33:25:48	16.02	5	-	-	-	-
171	MCG-05-32-055, 383 G 49	13:35:11.7	-33:37:09	12.79	-2	3925	27	0	s11
172		13:35:13.4	-34:08:33	16.12	5	-	-	-	-
173	B133515.2-344829 <sup>b</sup>	13:35:14.8	-34:48:20	15.67	5	15162	92	0	DPP
174		13:35:15.1	-34:08:06	15.58	5	-	-	-	-
175		13:35:15.3	-33:51:47	15.51	5	-	-	-	-
176		13:35:16.9	-33:39:22	16.34	-2	-	-	-	-
177		13:35:21.5	-33:29:11	16.06	5	-	-	-	-
178		13:35:29.4	-34:36:19	16.13	5	-	-	-	-
179		13:35:32.6	-34:35:06	16.19	5	-	-	-	-
180		13:35:34.6	-34:21:28	16.30	-3	-	-	-	-
181		13:35:37.6	-32:52:04	16.19	5	-	-	-	-
182		13:35:46.9	-33:05:54	14.75	5	12731	15	0	s7
183		13:35:48.4	-33:15:50	14.94	5	22237	66	0	s2
184		13:35:48.6	-33:13:12	16.30	5	-	-	-	-
185		13:36:02.8	-32:38:24	16.29	5	-	-	-	-
186		13:36:09.1	-32:38:25	16.10	-2	-	-	-	-
187		13:36:11.0	-32:39:17	16.16	-2	-	-	-	-
188		13:36:21.1	-32:57:09	15.80	5	-	-	-	-
189		13:36:25.2	-33:09:51	15.15	5	12660	53	8	s10
190		13:36:30.0	-34:06:25	15.61	5	-	-	-	-
191		13:36:33.5	-34:17:58	16.33	5	-	-	-	-
242	HSTGC 07274-00974 <sup>d</sup>	13:36:34.2	-34:01:07	15.85	5	-	-	-	-
192	383 G 55	13:36:34.7	-33:55:59	14.09	5	7691	10	0	MFB
193	B133644.2-334554 <sup>b</sup>	13:36:43.7	-33:45:47	15.43	5	15222	32	0	s6
194	383 G 56	13:36:45.2	-32:38:21	14.75	5	12260	30	4	s5
195		13:36:45.7	-33:55:19	15.66	5	-	-	-	-
196	B133656.1-332407 <sup>b</sup>	13:36:56.0	-33:24:01	14.62	5	15494	47	0	s2
197	B133656.6-324951 <sup>b</sup>	13:36:56.6	-32:49:51	15.42	5	15327	15	4	s10
199		13:37:04.7	-34:04:22	15.79	5	-	-	-	-
200	383 G 59	13:37:11.2	-32:38:32	15.43	5	7364	28	6	s5
201	B133712.1-324853 <sup>b</sup>	13:37:12.1	-32:48:53	15.89	5	11841	59	0	DPP
202		13:37:14.6	-33:50:08	16.05	5	-	-	-	-

Table 4—Continued

WMMA Id.	Identification	R.A.	Dec.	$R_F$	T	$v_{\odot}$	$\pm$	$N_e$	Ref
(1)	(2)	B1950.0 (3)	B1950.0 (4)	(5)	(6)	$\text{kms}^{-1}$ (7)	$\text{kms}^{-1}$ (8)	(9)	(10)
203		13:37:21.4	-33:40:28	14.67	5	15088	31	0	s2
204		13:37:34.6	-33:44:14	15.78	-2	–	–	–	–
205		13:37:35.9	-32:42:56	15.70	5	–	–	–	–
206	B133737.8-334408 <sup>b</sup>	13:37:37.8	-33:44:08	16.04	5	14867	61	0	DPP
207	MCG-05-32-063, 383 G 60	13:37:38.5	-33:24:09	12.81	5	3890	40	3	s1
208		13:37:39.8	-33:44:22	14.95	-3	14928	35	4	s7
209		13:37:45.6	-33:44:17	14.32	-3	14840	28	0	s7
210		13:37:45.8	-34:08:18	16.20	5	–	–	–	–
211		13:37:55.0	-34:06:26	15.82	5	–	–	–	–
212	B133801.9-332524 <sup>b</sup>	13:38:02.2	-33:25:19	15.57	5	15167	66	0	DPP
213		13:38:03.8	-33:04:57	14.59	5	12184	56	7	s9
214		13:38:07.7	-33:50:57	15.99	5	–	–	–	–
215		13:38:08.3	-33:56:00	15.61	5	–	–	–	–
216		13:38:10.1	-34:04:55	16.30	5	–	–	–	–
217	B133812.4-340713 <sup>b</sup>	13:38:12.9	-34:07:04	16.28	5	15485	98	0	DPP
218		13:38:13.9	-33:16:47	16.09	-2	–	–	–	–
219		13:38:16.3	-32:47:54	15.40	5	4494	44	8	s11
220		13:38:21.9	-34:35:37	16.32	5	–	–	–	–
221		13:38:26.4	-34:07:16	15.40	-2	16005	27	0	s10
222		13:38:28.5	-33:15:16	15.89	5	–	–	–	–
223		13:38:30.4	-34:38:14	15.64	-5	–	–	–	–
224		13:38:34.9	-34:06:53	15.08	5	16013	27	0	s8
225		13:38:39.3	-33:19:46	16.17	5	–	–	–	–
244		13:38:39.5	-33:41:15	17.13	-5	15288	32	0	s11
226	B133839.8-340745 <sup>b</sup>	13:38:40.4	-34:07:37	15.75	5	16922	36	0	s8
227	B133840.8-334114 <sup>b</sup>	13:38:41.0	-33:41:14	15.49	5	15425	44	6	s11
228		13:38:46.3	-34:13:12	15.65	5	–	–	–	–
230		13:38:47.7	-34:47:10	16.21	5	–	–	–	–
229		13:38:47.7	-34:03:40	16.34	5	–	–	–	–
231		13:38:48.4	-34:10:44	14.49	-5	15620	77	0	s1
232	B133849.2-334906 <sup>b</sup>	13:38:49.4	-33:49:05	15.96	5	14610	47	0	DPP
233		13:38:52.9	-33:57:47	15.56	5	–	–	–	–
234	B133857.2-325558 <sup>b</sup>	13:38:57.2	-32:56:02	15.63	5	11945	65	0	DPP
235		13:39:01.1	-33:50:50	15.59	-2	–	–	–	–
236		13:39:05.1	-33:19:43	15.65	5	–	–	–	–
238		13:39:06.2	-33:48:14	16.10	-2	–	–	–	–
237		13:39:06.2	-33:43:54	16.30	5	–	–	–	–
239		13:39:08.2	-33:05:30	16.02	5	–	–	–	–
240	383 G 63	13:39:10.6	-34:17:18	14.72	5	14547	28	7	s8

<sup>a</sup>Identification in Gregorini et al. (1994).

<sup>b</sup>Identification in Drinkwater et al. (1999).

<sup>c</sup>Identification in Arp & Madore (1987).

<sup>d</sup>Identification in Lasker et al. (1990).

<sup>e</sup>Identification in Quintana et al. (1995).

<sup>f</sup>Identification in Buta (1995).

<sup>g</sup>Galaxy identified by the Mount Stromlo Abell Cluster Supernova Search Team (1997)

References. — CFCQ: Cote et al. (1997) ; DC1: da Costa et al. (1986) ; DC2: da Costa et al. (1987); DC3: da Costa (1992), private communication; DPP: Drinkwater et al. (1999); MFB: Matthewson et al. (1992); QRM: Quintana et al. (1995).; T98: Theureau et al. (1998)

Table 5. Dynamical Parameters of Clusters

Parameter	Units	A3565	A3560
$\alpha$ (1950.0)		$13^h 33^m 04^s \pm 4^s$	$13^h 30^m 12^s \pm 2^s$
$\delta$ (1950.0)		$-33^\circ 31' 50'' \pm 49''$	$-32^\circ 53' 26'' \pm 20''$
$l$		$313.41^\circ$	$312.87^\circ$
$b$		$28.18^\circ$	$28.92^\circ$
$N_g$		29	32
$v_\odot$	$\text{kms}^{-1}$	$3759 \pm 9$	$14645 \pm 20$
$v_0$	$\text{kms}^{-1}$	$3567 \pm 9$	$14452 \pm 20$
$\sigma$	$\text{kms}^{-1}$	$228 (+38, -26)$	$588 (+92, -63)$
$v_{bi-weight}$	$\text{kms}^{-1}$	$3586 \pm 45$	$14470 \pm 123$
$\sigma_{bi-weight}$	$\text{kms}^{-1}$	$236 \pm 69$	$614 \pm 68$
$R_h$	$h^{-1} \text{Mpc}$	$0.37 \pm 0.01$	$0.34 \pm 0.09$
$R_p$	$h^{-1} \text{Mpc}$	$0.53 \pm 0.03$	$1.03 \pm 0.04$
$t_c$	Hubble times	0.04	0.02
$M_{VT}$	$h^{-1} M_\odot$	$2.72 (+1.01, -0.71) \times 10^{13}$	$1.64 (+0.93, -0.77) \times 10^{14}$
$M_p$	$h^{-1} M_\odot$	$3.29 \pm 0.17 \times 10^{13}$	$4.90 \pm 0.19 \times 10^{14}$
(M/L)	(M/L) $_\odot$	143	760

Table 6. Additional radial velocities

Gal Id.	Other Id.	R.A.	Dec.	$v_{\odot}$	$\pm$
(1)	(2)	B1950.0	B1950.0	$\text{kms}^{-1}$	$\text{kms}^{-1}$
		(3)	(4)	(5)	(6)
HSTGC 07272-01686		13:21:56.0	-34:02:46	15074	25
HSTGC 07268-00028		13:22:17.0	-33:05:27	13783	26
HSTGC 07272-00317	382 G 60	13:22:37.0	-33:32:12	8004	22
HSTGC 07268-01809	MGP 1133 <sup>a</sup>	13:23:59.0	-31:44:14	14008	51
HSTGC 07268-01860	MGP 1145 <sup>a</sup>	13:24:03.0	-31:44:56	14792	31
HSTGC 07272-00553		13:24:58.0	-33:44:35	15023	26
HSTGC 07268-02068	383 G 01	13:25:14.0	-33:25:52	8091	16
HSTGC 07272-00677		13:25:19.0	-33:46:53	14426	26
HSTGC 07268-01590	MGP 2691 <sup>a</sup>	13:27:06.0	-31:53:01	3886	40
HSTGC 07265-01949	444 G 60	13:27:43.0	-31:19:06	14489	29
HSTGC 07269-00325	MGP 2953 <sup>a</sup>	13:27:44.0	-32:00:24	4044	20
HSTGC 07277-01636		13:28:11.0	-35:54:12	7218	34
HSTGC 07269-00374	MGP 3249 <sup>a</sup>	13:28:30.0	-31:48:39	12956	23
WMMA 248 <sup>b</sup>		13:28:44.8	-32:45:13	13697	57
HSTGC 07269-01680		13:28:45.0	-32:43:27	3579	31
HSTGC 07269-01750	AM 1328-325 <sup>c</sup>	13:28:49.0	-32:59:08	16579	35
HSTGC 07269-01424	383 G 12	13:28:52.0	-33:07:23	7738	21
HSTGC 07269-00860		13:28:56.0	-32:38:15	14780	48
HSTGC 07269-01083NW		13:29:23.6	-32:34:30	14017	24
HSTGC 07269-01083SE		13:29:24.0	-32:34:33	14366	25
HSTGC 07269-00070	444 G 70	13:29:56.0	-31:42:35	11106	31
HSTGC 07273-01687	IRAS 13321-3514 <sup>d</sup>	13:32:06.0	-35:14:35	15840	29
WMMA 246 <sup>e</sup>		13:32:45.0	-33:16:34	65529	71
HSTGC 07269-01344		13:33:05.0	-32:30:14	7483	38
HSTGC 07273-01829		13:33:28.0	-34:51:28	4267	30
WMMA 247 <sup>f</sup>		13:34:06.3	-33:29:36	11479	49
HSTGC 07269-00876	CSRG 0732 <sup>g</sup>	13:34:21.0	-32:12:21	13660	50
HSTGC 07265-02190		13:34:48.0	-31:31:20	11831	28
HSTGC 07273-00119	AM 1334-351 <sup>c</sup>	13:34:55.0	-35:14:50	15268	24
HSTGC 07277-00869	383 G 47	13:34:57.0	-35:47:46	3629	21
HSTGC 07266-00111	CSRG 0737 <sup>g</sup>	13:36:30.0	-31:25:26	11574	25
HSTGC 07266-00139	IRAS 13365-3116 <sup>d</sup>	13:36:31.0	-31:16:40	6932	47
HSTGC 07270-00593	445 G 03	13:36:41.0	-31:51:03	6969	43
HSTGC 07278-01640	PL 1 <sup>h</sup>	13:37:19.0	-35:25:19	15638	52
HSTGC 07270-00628		13:37:52.0	-31:53:58	11784	25
HSTGC 07270-00562	445 G 09	13:37:57.0	-32:24:18	11436	27
HSTGC 07270-00284		13:38:03.0	-33:04:55	12155	116
HSTGC 07270-00724	445 G 11	13:38:35.0	-31:45:01	6634	60
HSTGC 07274-01160		13:39:49.0	-33:44:39	5726	31
HSTGC 07278-01018	383 G 62A	13:39:03.0	-35:26:50	11467	33
HSTGC 07278-01224	383 G 62	13:39:02.4	-35:26:35	8789	37
HSTGC 07278-01206	383 G 64	13:39:13.0	-36:05:50	11474	44
HSTGC 07270-00993		13:40:07.0	-31:38:04	11639	29
HSTGC 07274-01486		13:40:26.0	-33:51:32	15073	40
HSTGC 07278-01133		13:40:41.0	-36:09:57	4285	41
HSTGC 07266-00818		13:42:12.0	-31:23:01	4678	37
HSTGC 07270-02135	383 G 73	13:42:20.0	-33:25:44	11851	26
HSTGC 07270-01022		13:42:24.0	-32:23:49	9665	28
HSTGC 07270-02249		13:43:42.0	-33:17:30	7521	29
HSTGC 07270-01038		13:44:37.0	-31:53:31	12749	37
HSTGC 07274-00031	383 G 80	13:44:50.0	-34:43:13	11504	23
HSTGC 07270-01147	445 G 33	13:45:00.0	-32:12:46	12229	29
HSTGC 07283-00985		13:45:13.0	-32:15:36	11745	29
HSTGC 07279-01872	IRAS F13454-3132 <sup>d</sup>	13:45:24.0	-31:31:50	11428	42

<sup>a</sup>Identification in Metcalfe, Godwin & Peach (1994).

<sup>b</sup>The galaxy wmma 248 is a background object some  $2'$  to the south of HSTGC 07269-01680.

<sup>c</sup>Identification in Arp & Madore (1987).

<sup>d</sup>Identification in IRAS Faint Source Catalog.

<sup>e</sup>Serendipitous galaxy located between WMMA 117 and WMMA 245 of Table 4. Coordinates estimated from the Digital Sky Survey.

<sup>f</sup>Serendipitous galaxy located between WMMA 145 and WMMA 147.

<sup>g</sup>Identification in Buta (1995).

<sup>h</sup>Identification in Postman & Lauer (1995).



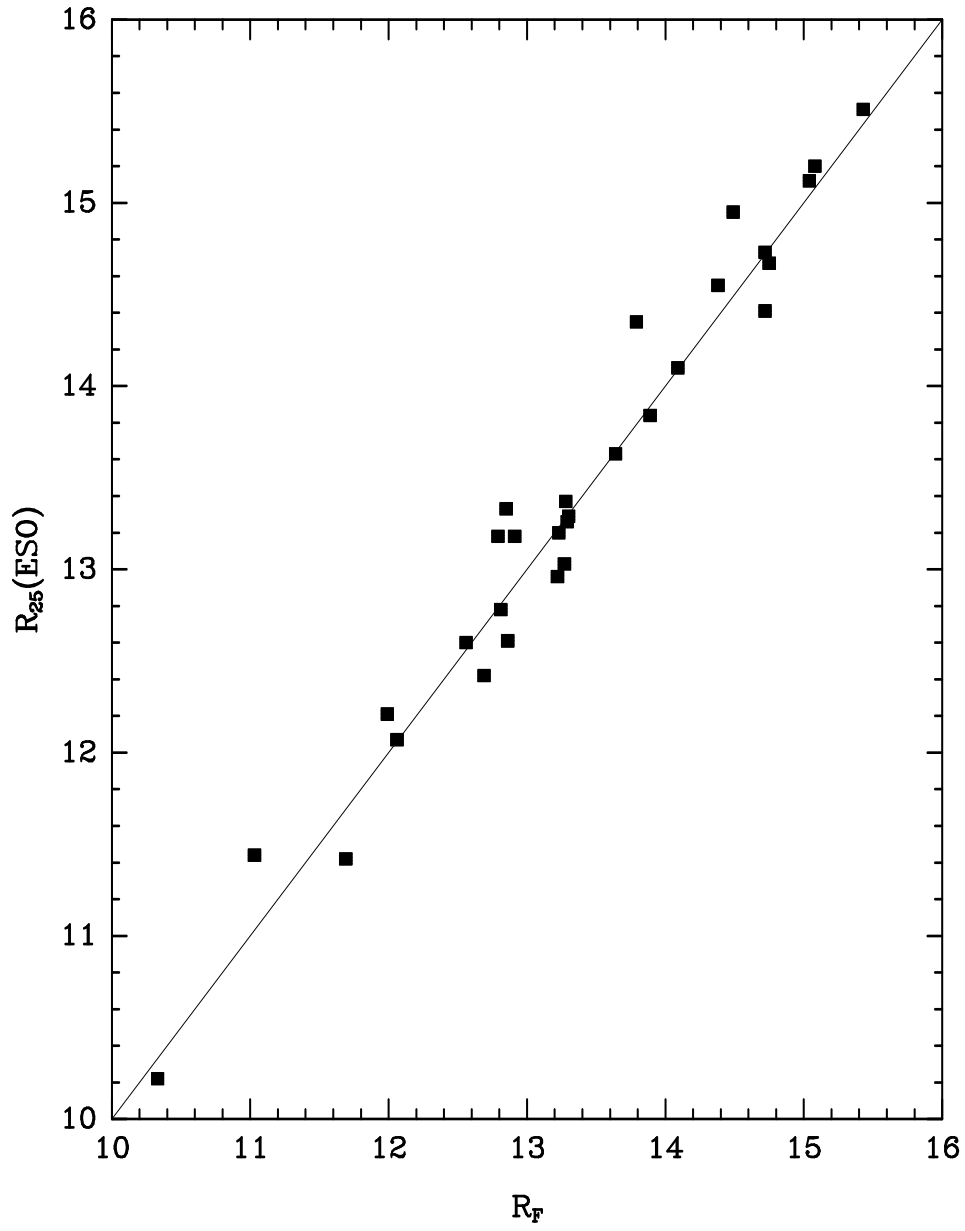


Fig. 1.— Comparison between our  $R_F$  magnitudes and  $R_{25}(ESO)$  from ESO-IV.

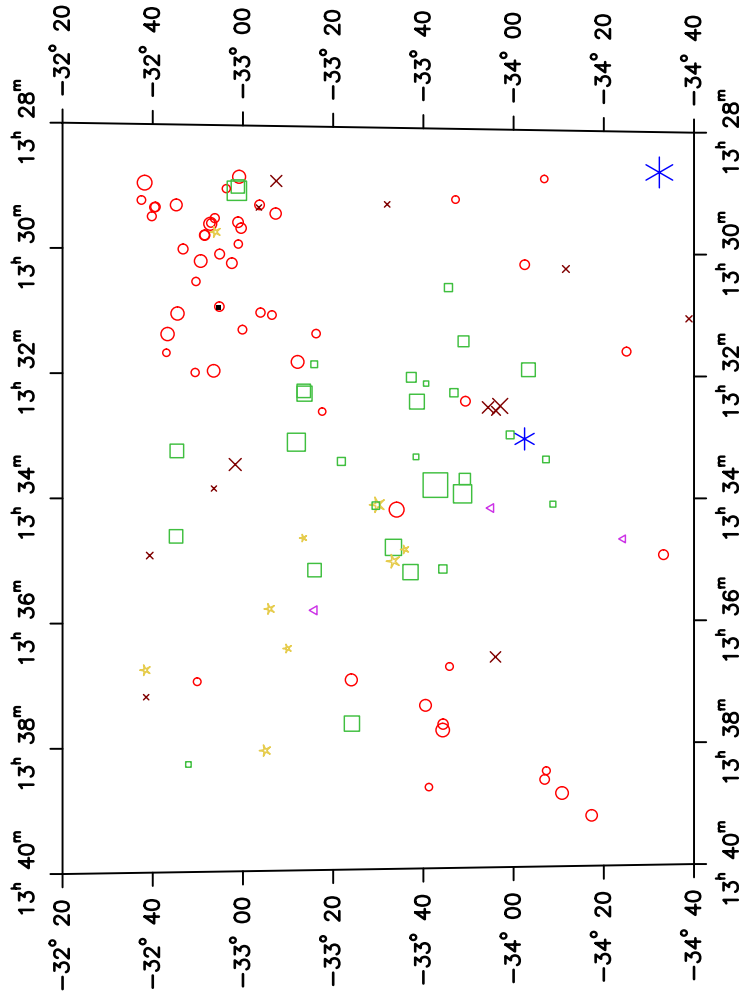


Fig. 2.— Distribution of galaxies within the surveyed region with  $R_F \leq 15.50 \text{ mag}$ . The symbol sizes represent the apparent magnitude of galaxies. The solid square represents the galaxy without a redshift measurement, while the remaining symbols correspond to the following intervals: asterisks ( $v \leq 3000 \text{ km s}^{-1}$ ); open squares ( $3000 < v \leq 5000 \text{ km s}^{-1}$ ); crosses ( $5000 < v \leq 10000 \text{ km s}^{-1}$ ); stars ( $10000 < v \leq 13000 \text{ km s}^{-1}$ ); open circles ( $13000 < v \leq 17000 \text{ km s}^{-1}$ ) and open triangles ( $v > 17000 \text{ km s}^{-1}$ ).

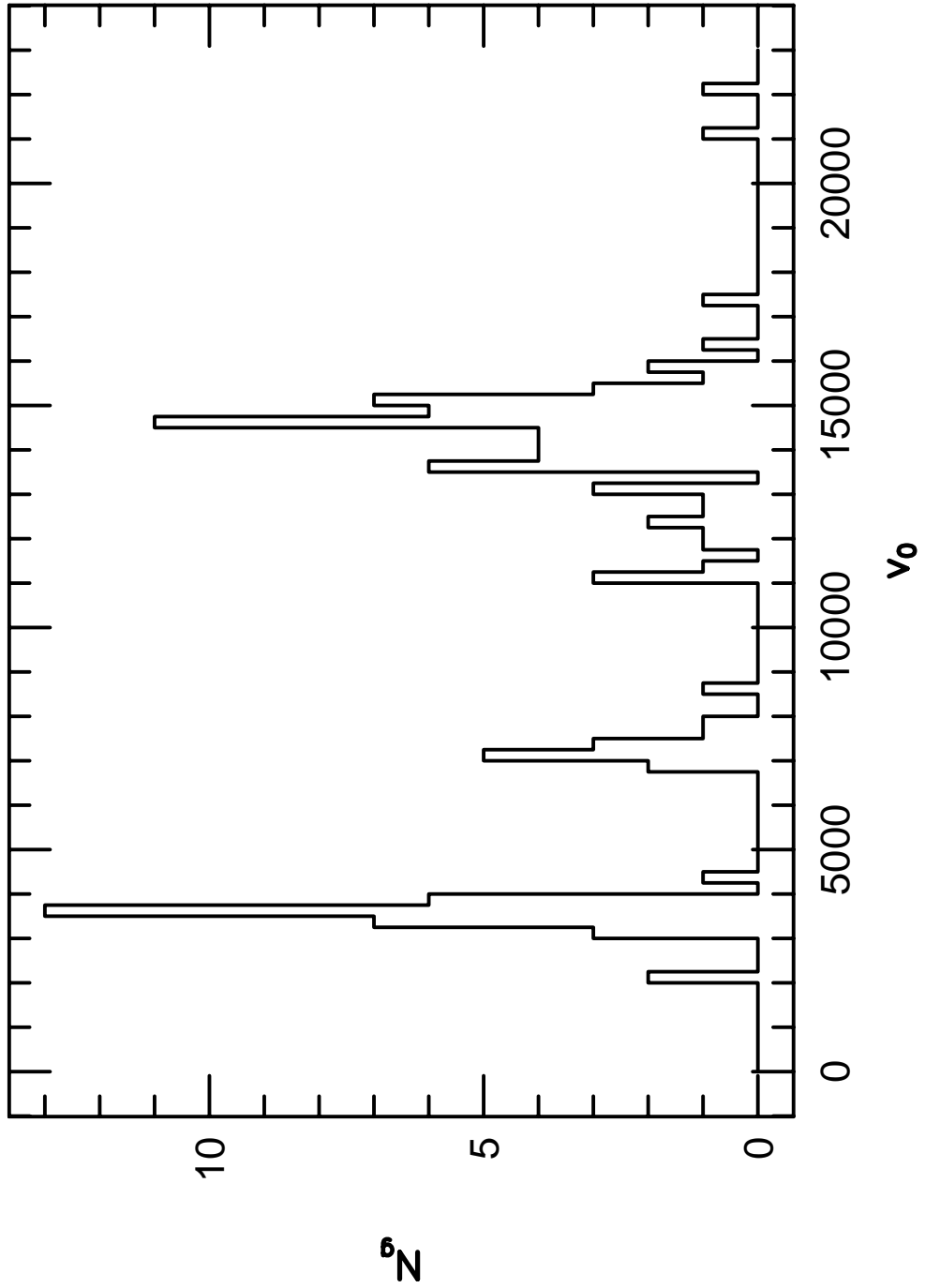


Fig. 3.— Distribution of radial velocities of galaxies corrected for galactic rotation within the surveyed region, in bins of  $250 \text{ kms}^{-1}$ .

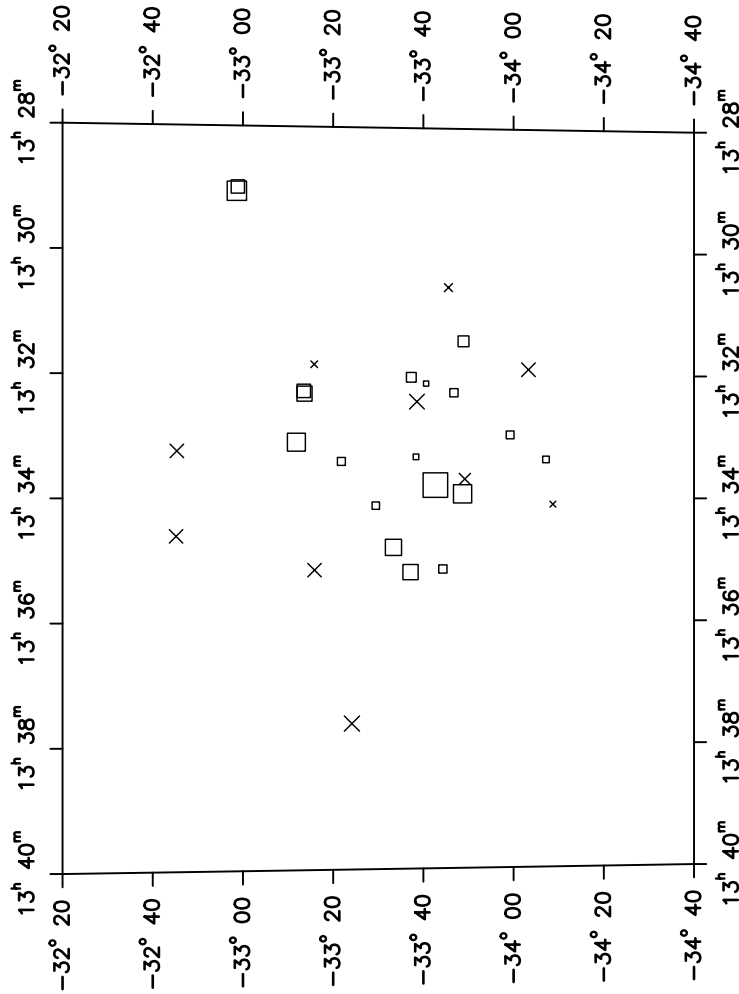


Fig. 4.— Distribution of galaxies within 3000 and 5000  $\text{kms}^{-1}$ . Open squares represent galaxies with absorption line spectra and crosses galaxies with emission lines.

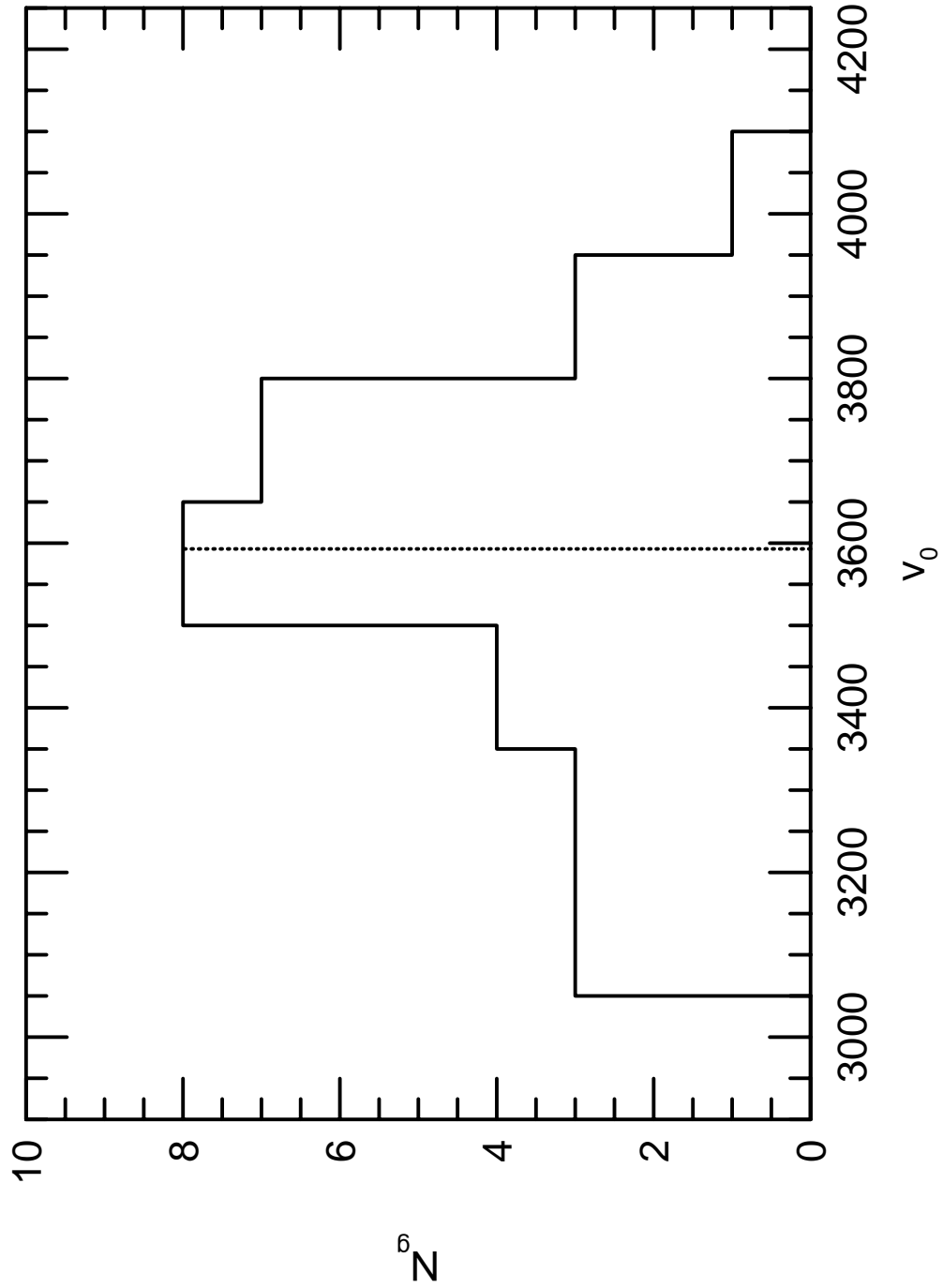


Fig. 5.— Distribution of radial velocities of galaxies of A3565, corrected for galactic rotation. The bin size is  $150 \text{ km s}^{-1}$ ; the dotted line represents the radial velocity of IC 4296.

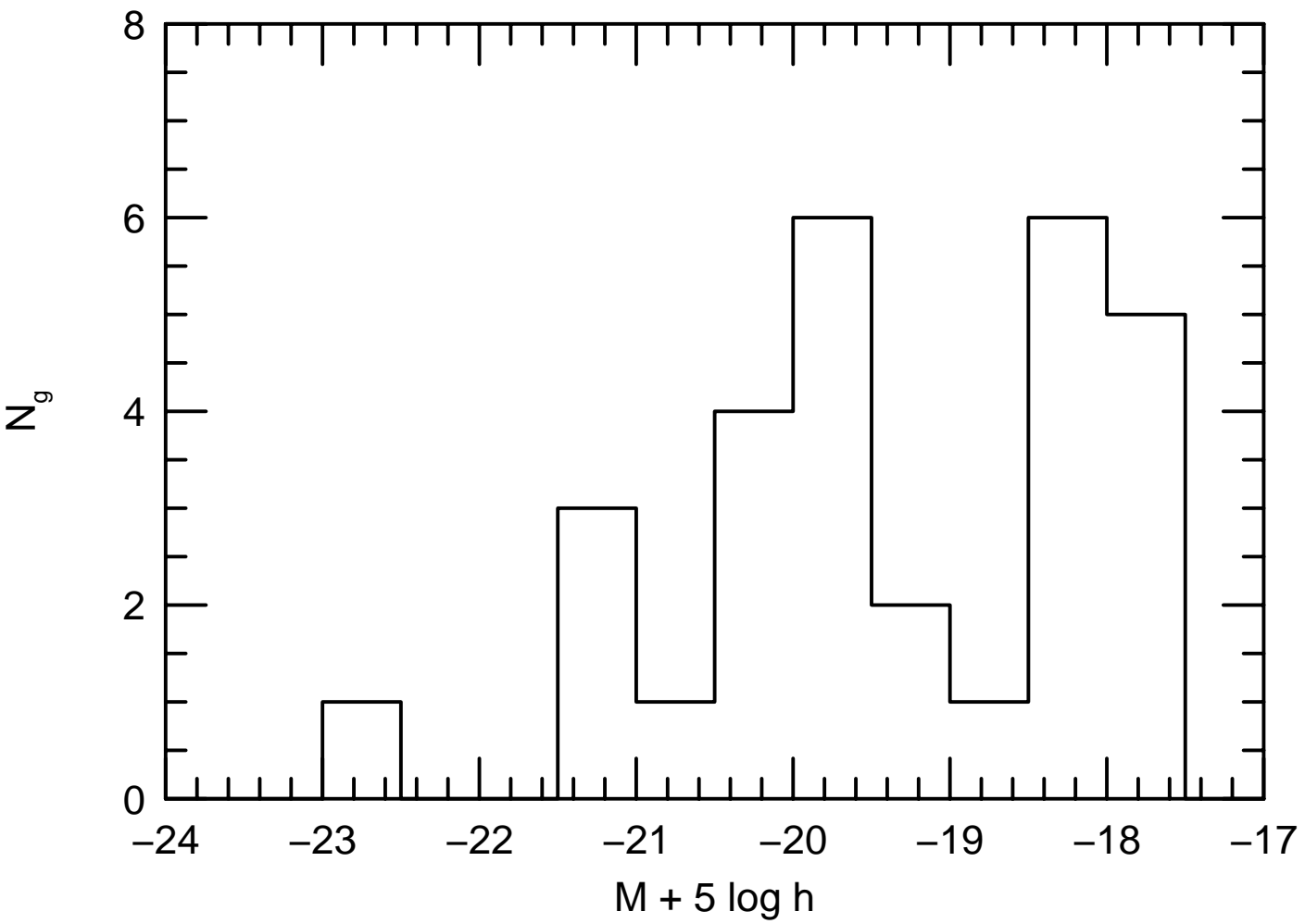


Fig. 6.— Distribution of absolute magnitudes of A3565 galaxies in 0.5 *mag* bins. The absolute magnitudes were calculated using the mean group velocity.

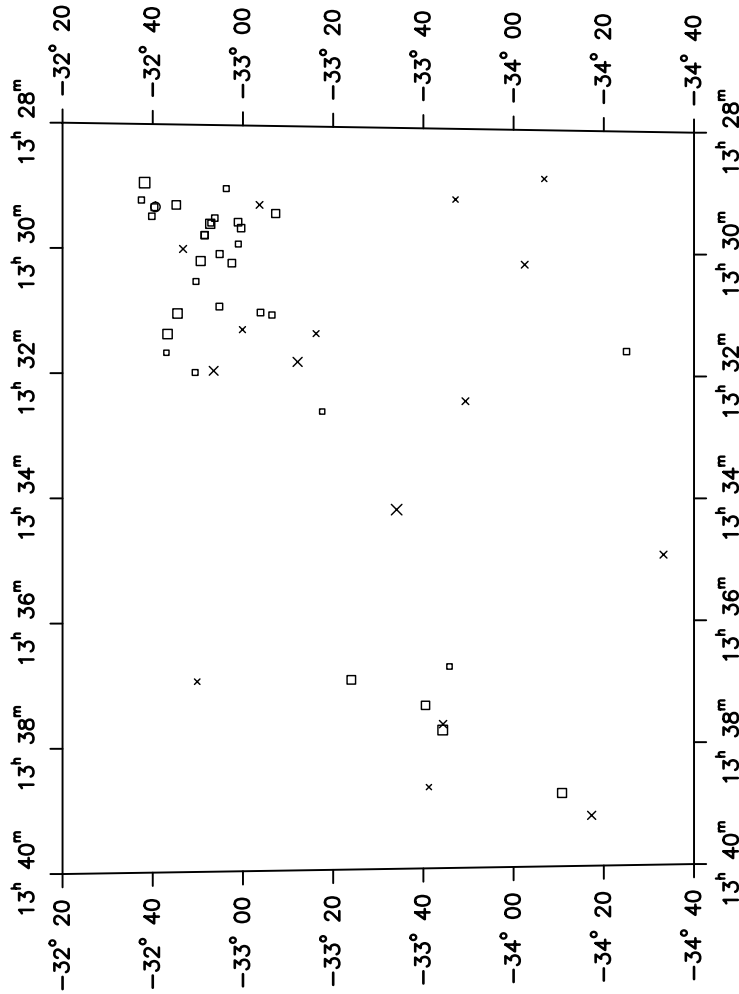


Fig. 7.— Distribution of galaxies in the radial velocity interval  $13000 \text{ km s}^{-1} \leq v_0 \leq 16000 \text{ km s}^{-1}$ . Galaxies with absorption-line spectra are represented by open squares and emission-line galaxies are shown as crosses. The open circle represent the galaxy whose spectrum could not be inspected. As for A3565, there are very few galaxies with emission lines in A3560, most of them being found in the outer regions of the cluster.

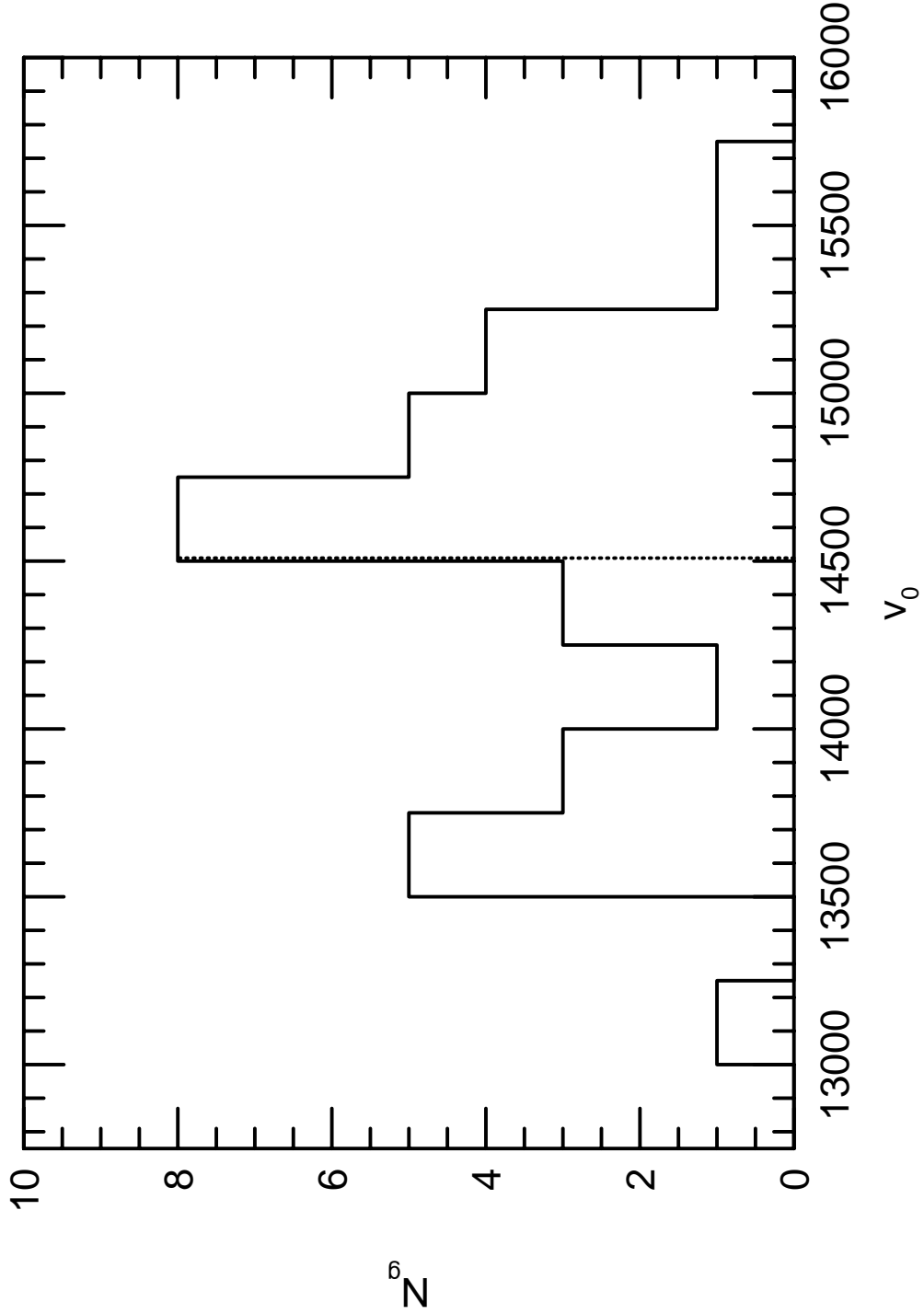


Fig. 8.— Radial Velocity distribution of galaxies in the region  $13^h 28^m \leq \alpha \leq 13^h 33^m$  and  $-33^\circ 30' \leq \delta \leq -32^\circ 20'$ , in  $250 \text{ km s}^{-1}$  bins. The dotted line shows the radial velocity of the dumbbell galaxy formed by objects WMMA 032 and WMMA 033 in Table 4.



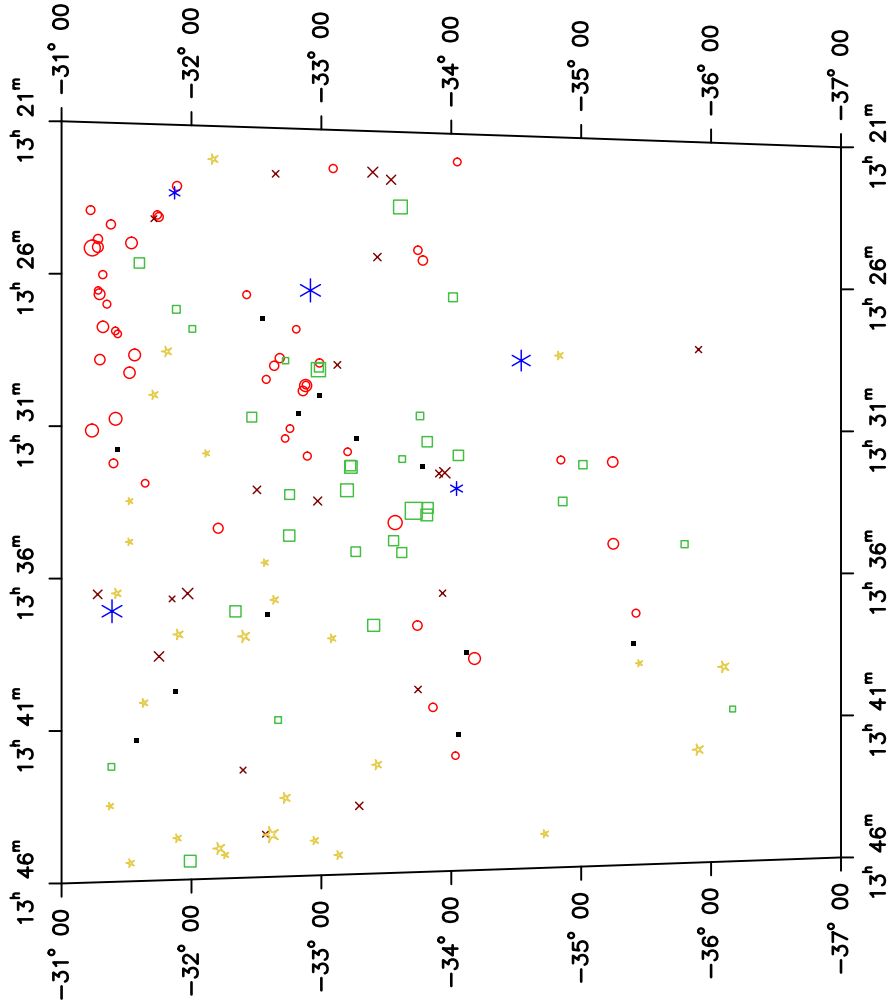


Fig. 9.— Distribution of galaxies brighter than  $m_B = 15.5 \text{ mag}$  in a  $5^\circ \times 5^\circ$  region centered on IC 4296. The symbols have the same meaning as in Figure 2. The figure shown no significant increase in the number of galaxies in the redshift interval of 3000 to 5000  $\text{kms}^{-1}$  (open squares) which could belong to A3565.